

ABSOLUTE CALIBRATION AND CHARACTERIZATION OF THE MULTIBAND IMAGING PHOTOMETER FOR SPITZER. I. THE STELLAR CALIBRATOR SAMPLE AND THE 24  $\mu$ m CALIBRATIONC. W. Engelbracht<sup>1</sup>, M. Blaylock<sup>1</sup>, K. Y. L. Su<sup>1</sup>, J. Rho<sup>2</sup>, G. H. Rieke<sup>1</sup>, J. Muzerolle<sup>1</sup>, D. L. Padgett<sup>2</sup>, D. C. Hines<sup>3</sup>, K. D. Gordon<sup>1</sup>, D. Fadda<sup>2</sup>, A. Noriega-Crespo<sup>2</sup>, D. M. Kelly<sup>1</sup>, W. B. Latter<sup>4</sup>, J. L. Hinz<sup>1</sup>, K. A. Misselt<sup>1</sup>, J. E. Morrison<sup>1</sup>, J. A. Stansberry<sup>1</sup>, D. L. Shupe<sup>2</sup>, S. Stolovy<sup>2</sup>, W. M. A. Wheaton<sup>2</sup>, E. T. Young<sup>1</sup>, G. Neugebauer<sup>1</sup>, S. W. Achter<sup>2</sup>, P. G. Perez-Gonzalez<sup>1,5</sup>, D. T. Frayer<sup>2</sup>, and F. R. Marleau<sup>2</sup>

Draft version August 30, 2016

## ABSTRACT

We present the stellar calibrator sample and the conversion from instrumental to physical units for the 24  $\mu$ m channel of the Multiband Imaging Photometer for Spitzer (MIPS). The primary calibrators are A stars, and the calibration factor based on those stars is  $4.54 \times 10^{-2} \text{ M Jy sr}^{-1} (\text{DN/s})^{-1}$ , with a nominal uncertainty of 2%. We discuss the data-reduction procedures required to attain this accuracy; without these procedures, the calibration factor obtained using the automated pipeline at the Spitzer Science Center is 1.6%–0.6% lower. We extend this work to predict 24  $\mu$ m flux densities for a sample of 238 stars which covers a larger range of flux densities and spectral types. We present a total of 348 measurements of 141 stars at 24  $\mu$ m. This sample covers a factor of  $\sim 460$  in 24  $\mu$ m flux density, from 8.6 mJy up to 4.0 Jy. We show that the calibration is linear over that range with respect to target flux and background level. The calibration is based on observations made using 3-second exposures; a preliminary analysis shows that the calibration factor may be 1% and 2% lower for 10- and 30-second exposures, respectively. We also demonstrate that the calibration is very stable: over the course of the mission, repeated measurements of our routine calibrator, HD 159330, show a root-mean-square scatter of only 0.4%. Finally, we show that the point spread function (PSF) is well measured and allows us to calibrate extended sources accurately; Infrared Astronomy Satellite (IRAS) and MIPS measurements of a sample of nearby galaxies are identical within the uncertainties.

Subject headings: infrared: stars| instrumentation: detectors

## 1. INTRODUCTION

Space-based infrared astronomy satellites have used a variety of methods to perform flux calibration. For example, the Infrared Astronomy Satellite (IRAS; Beichman et al. 1988) extrapolated a ground-based 10  $\mu$ m calibration out to 60  $\mu$ m using stellar models and then used asteroids to transfer the 60  $\mu$ m calibration to 100  $\mu$ m. The Midcourse Space Experiment (MSX) was calibrated in a set of bands from 8–20  $\mu$ m using blackbodies ejected from the spacecraft itself (Price et al. 2004). The instruments aboard the Infrared Space Observatory (ISO) used a mix of astronomical sources, from stars for the ISO Camera (ISOCAM; Blommaert et al. 2003) to stars, asteroids, and planets for the ISO Photometer (ISOPHOT; Schulz et al. 2002) and Short Wavelength Spectrometer (SWIS; Decin et al. 2000) and planets for the Long Wavelength Spectrometer (LWS; Gory et al. 2003). The Deep Infrared Background Experiment (DIRBE) imaged the sky in a series of bands from 1.25  $\mu$ m to 240  $\mu$ m and was

calibrated against stars, planets, and planetary nebulae (Hauser et al. 1998). Like most of these missions, the instruments on board the Spitzer Space Telescope (Werner et al. 2004) are calibrated against celestial sources: for example, the Infrared Array Camera (IRAC; Fazio et al. 2004), with photometric bands from 3–8  $\mu$ m, is calibrated against stars (Reach et al. 2005), as is the Infrared Spectrograph (IRS; Houck et al. 2004).

The Multiband Imaging Photometer for Spitzer (MIPS; Rieke et al. 2004) has three photometric bands at 24, 70, and 160  $\mu$ m. Like the other Spitzer instruments, the primary flux calibrators at 24 and 70  $\mu$ m are stars; the calibrations are tied to the new infrared calibration by Rieke et al. (2007) and are presented here (24  $\mu$ m) and in a companion paper by Gordon et al. (2007) (70  $\mu$ m). The sensitivity of the 160  $\mu$ m band is sufficient to allow it to be calibrated against stars, too, but a strong, short-wavelength ghost image limits the accuracy with which such hot sources can be measured; hence, an asteroid-based transfer (and the color corrections required to make the transfer) of the stellar calibration from the shorter bands (similar in spirit to the IRAS 100  $\mu$ m calibration) is presented in a companion paper by Stansberry et al. (2007).

The MIPS 24  $\mu$ m calibration and capabilities can be compared to several previous missions which overlap in wavelength. For example, the quoted absolute calibration uncertainties of the large surveys performed by IRAS at 25  $\mu$ m, by MSX at 21  $\mu$ m and by DIRBE at 25  $\mu$ m are 8% (Beichman et al. 1988), 7% (Cohen et al. 2001), and 15% (Hauser et al. 1998), respectively. These missions were optimized for large area surveys and used

<sup>1</sup> Steward Observatory, University of Arizona, Tucson, AZ 85721; cengelbracht, mblaylock, ksu, griek, muzerolle, kgordon, dkelly, jhinz, kmiselt, jmorrison, jstansberry, eyoung, gxn@as.arizona.edu

<sup>2</sup> Spitzer Science Center, 220-6, Caltech, Pasadena, CA 91125; rho, dlp, fadda, alberto, shupe, stolovy, waw, wachter, frayer, marleau@ipac.caltech.edu

<sup>3</sup> Space Science Institute, 4750 Walnut Street, Suite 205, Boulder, CO 80301; dhines@as.arizona.edu

<sup>4</sup> NASA Herschel Science Center, Mail Code 100-22, California Institute of Technology, 770 South Wilson Avenue, Pasadena, CA 91125; latter@ipac.caltech.edu

<sup>5</sup> current address: Departamento de Astronómica, Facultad de Ciencias, Universidad Complutense de Madrid, E-28040 Madrid, Spain; pperez@as.arizona.edu

older detector technology. As a result, the beam size and point source detection limits are poor compared to the Spitzer and ISO pointed observatories. Like MIPS, the ISOPHOT instrument was designed as a general user instrument, but the 25  $\mu\text{m}$  channel (which achieved an accuracy of  $\sim 10\%$ ; Klaas et al. 2003) was an aperture photometer and not capable of imaging. Thus, MIPS is the first space instrument with an array detector optimized for imaging near 24  $\mu\text{m}$ , achieving a point-source sensitivity of  $\sim 60$  Jy (5  $\sigma$ , 2000 seconds; Spitzer Observer's Manual), with a beam of  $6''$  FWHM. As we show in this paper, the absolute calibration of the MIPS 24  $\mu\text{m}$  channel is accurate to 2%, which has expanded the science possible in this wavelength range. For example, the MIPS 24  $\mu\text{m}$  channel allows measurement of infrared excesses around stars with lower effective temperatures and/or lower-mass debris disks than previously possible (e.g., Rieke et al. 2005; Bryden et al. 2006).

Careful data reduction procedures are essential to reproduce the results presented here; accordingly, we discuss the data reduction and photometry in some depth in §2. The calibration factor itself is computed in §3. To explore the quality of the calibration, we expand the sample of targets beyond those used to measure the calibration factor; the details of the flux prediction are presented in §4. We use the expanded sample in a series of tests of the calibration, discussed in §5. Finally, we summarize our results in §6.

## 2. DATA REDUCTION AND PHOTOMETRY

### 2.1. Standard Processing

The data were all obtained using the MIPS small-field photometry mode astronomical observation template (AOT). For most targets, 2 cycles of photometry using 3-second exposures were obtained, resulting in 14 individual images at each of 2 telescope nod positions (excluding the short exposure that starts the data-taking sequence at each of the two telescope nod positions). Starting with the raw data downloaded from the Spitzer Science Center (SSC), these data were processed using version 3.06 of the MIPS Data Analysis Tool (DAT; Gordon et al. 2005), which performs standard processing of infrared detector array data (slope fitting, dark subtraction, linearity correction, flat fielding, and mosaicking) as well as steps specific to the array used in MIPS (droop correction and dynamic range extension using the first difference frame). These steps are described in more detail in that paper. Experience gained with the flight instrument has prompted the application of additional processing, not discussed by Gordon et al. (2005), to remove low-level instrumental artifacts. In particular, one of the four readouts on the array can incur an offset of several counts per second (due to a bright source or cosmic ray on detectors connected to that readout) relative to the other three, resulting in a striping effect (dubbed "jailbar"); an additive correction is applied to that readout to remove the effect. Also, the in-orbit flat field has several dark spots (due to particulate matter on the pick-off mirror) that shift position on the array as the scan mirror (which imposes small pointing adjustments as part of the normal observing sequence) moves. To remove these spots, a flat field specific to scan mirror position is applied as part of the standard processing. These artifacts are illustrated in Figure 1.

### 2.2. Additional Processing

There are additional low-level artifacts present in the MIPS data after the standard processing described above has been applied. We assess the severity of these effects and correct those that impact significantly our measurements. In roughly decreasing order of importance, these artifacts are:

The MIPS 24  $\mu\text{m}$  array is subject to medium-term ( $\sim 1$  week) gain changes that affect pixels which have been exposed to highly saturating sources, at the level of a few percent. A typical MIPS 24  $\mu\text{m}$  observation will have several regions that have been affected this way as the cumulative result of normal operations during that instrument campaign. An additional flat field, made from a median stack of the data with the source masked out, is applied to remove the gain changes.

Background levels observed by MIPS at 24  $\mu\text{m}$  can change by several counts per second from image to image throughout an observing sequence, likely due to scattered zodiacal light that depends on the position of the MIPS scan mirror. Uncorrected, this can affect the photometry of our faintest ( $\sim 10$  mJy) calibrators at the level of about a percent. To mitigate this effect, we subtract the median level (after masking the source) from each image before mosaicking.

Any source that falls on the MIPS 24  $\mu\text{m}$  array leaves a residual image of about 0.5% that decays with a timescale of roughly 10 seconds. The dither pattern used in the photometry AOT ensures that the source falls on a different part of the array after every exposure, and thus any residual image has decayed to a small fraction of a percent by the time the new source position is within several full-width-half-maxima of a previous position. Residual images have a negligible effect on the calibration factor we derive here, and we perform no correction for them.

Sources that saturate the MIPS 24  $\mu\text{m}$  array in the full (3-second) exposures used here can affect the offset of the pixels read out after the ones on the source, and can even change the magnitude of the "jailbar" effect on those pixels, resulting in a different striping pattern above and below the source on the array. The offset is a few counts per second and only occurs for the brightest sources, so it has a negligible effect on the photometry of those sources and we make no correction here.

Examples showing the artifacts discussed here are shown in Figure 2.

### 2.3. Mosaicking

After applying the corrections discussed above, we coadd the data to make a mosaic image of each source. As the natural unit of a flat-fielded image is surface brightness, the mosaicking step conserves surface brightness as it removes optical distortions. The final images have square pixels  $2''.45$  on a side, very similar to the natural pixel width near the center of the array,  $2''.49$ . The source positions in the photometry AOT range over the central  $2.5''$  of the array; to ensure that there are no calibration changes across the full array, we have tested the distortion correction on individual images. Using the "phot" task in the Image Reduction and Analysis Facility (IRAF<sup>6</sup>), we compared photometry in a fixed aperture (6

<sup>6</sup> IRAF is distributed by the National Optical Astronomy Observatories, which are operated by the Association of Universities

pixels in radius, with a background annulus from 7–12 pixels) for 416 measurements of HD 042082 made during a focal plane survey which positioned the star over the full extent of the array. Without correction for distortion, the measured counts increased smoothly by 12% from the upper-left-hand corner of the array to the lower-right-hand corner of the array, inversely proportional to the 12% change in pixel area, from 6.91 square arcseconds to 6.11 square arcseconds. As expected, correcting the images for distortion eliminates this trend, resulting in a 1 $\sigma$  dispersion in the measurements of only 0.8%.

#### 2.4. Photometry

To compute aperture corrections for photometry, we make use of a point response function (PRF) constructed as follows. We start with a point spread function (PSF) of a 10000 K blackbody (the spectral energy distributions of the stars we use to calibrate differ negligibly from this at 24  $\mu$ m) generated using the Spitzer TinyTim software (TinyTim; Krist 2002). The PSF is computed at the center of the array using an image size (10 $^0$  width) large enough to encompass > 99% of the light. We observe the model using the MIPS simulator (software designed to simulate MIPS data, including optical distortions, using the same observing templates used in flight) and mosaic the simulated data using the same software with which we processed the real data. We compare the result to one of the calibration stars in Figure 3. The structure predicted by the model, down to very faint levels and in the diffraction spikes, is very similar to what is observed on a real star. Additional insight is gained from a comparison of radial profiles (Figure 4), where it can be seen that the model is an excellent description of the data, out to the third Airy ring. A similar, and slightly improved, fit to the radial profile can be obtained by smoothing the TinyTim model by the equivalent of a boxcar 1.8 pixels in width (possibly indicating a small amount of pointing jitter or scattered light, neither of which is modeled by the simulator). We apply the `\phot` task in IRAF to the boxcar-smoothed image to compute the aperture corrections, representative values of which are shown in Table 1. We find that the counts measured by various photometry routines vary by about a percent, so we assign a 1% uncertainty to the aperture correction.

We perform aperture photometry on the observations using an aperture 35 $^0$  in radius, with a background annulus from 40 $^0$  to 50 $^0$  in radius. This aperture is large enough to minimize uncertainties due to centroiding errors, and to ensure that any uncertainties in the aperture correction have a small effect on the derived counts. We derive the uncertainty on each measurement from the scatter of the pixel values in the background aperture. The measurements are listed in Table 2.

#### 2.5. Comparison to SSC Pipeline

We compare the measurements made on data reduced using the DAT to those obtained using identical photometry procedures on data processed using the automated pipeline at the SSC, which does not apply the second field (made using a median stack of the data; see x 2.2) or the background subtraction. We convert the units of the

SSC data products from M Jy/sr to DN/s by dividing by the FLUXCONV value found in the header. Based on 90 measurements of HD 159330 processed using the S15.3.0 version of the pipeline, we find that the count rate in the pipeline-reduced data is 1.6%  $\pm$  0.6% higher than in data reduced using the DAT. The difference between the reductions is marginally significant (2:7) and may be due to the extra processing steps applied to the DAT-processed data.

#### 2.6. Scan Map Calibration

The results we present here rely on measurements of calibrator stars performed using the photometry AOT, which images the sky in a nod-and-stare pattern. MIPS has a second imaging mode, the scan map AOT, which images the sky using a continuous track of the spacecraft. The scan mode uses the same optical train as the photometry mode and so we expect that the calibration derived here would apply equally to both modes. To check whether subtle differences exist in the shape of the PSF that might affect the calibration, we compare photometry in scan and photometry modes on two stars observed in multiple epochs, HD 159330 and HD 163588. We find that the radial profiles in scan and photometry modes are identical within the uncertainties and that photometry in these two modes agrees within 1%, confirming that the photometry calibration is applicable to scan-mode data. Similar results were found by Fadda et al. (2006).

### 3. THE 24 $\mu$ m CALIBRATION FACTOR

Following Rieke et al. (2007), we base the flux calibration of the MIPS 24  $\mu$ m band on A stars. We adopt the sample of 22 A stars from Rieke et al. (2007), as a consistent suite of measurements is available for these targets and the sample has already been vetted for sources which would bias the calibration, such as those with an infrared excess. Here and throughout this work, monochromatic flux densities are computed at 23.675  $\mu$ m, the effective wavelength of the 24  $\mu$ m band, although we will continue to use the shorthand "24  $\mu$ m" for convenience. We compute 24  $\mu$ m flux densities using the extinction-corrected  $K_s$  magnitudes computed by Rieke et al. (2007), a  $K_s$  [24] color difference of 0 magnitudes, and the 24  $\mu$ m (i.e., 23.675  $\mu$ m) zero point derived by Rieke et al. (2007), 7.17 Jy. We apply the aperture correction derived in x 2 (1.08) to the measurements from Table 2, averaging multiple measurements when available. The counts in that table are integrations over an aperture, so we convert the implied unit of "pixel" (that we have ignored thus far) to an angular area using the pixel size (2 $^0$ .45 on a side) of our mosaics. The calibration factor is the weighted average of the ratio of the 24  $\mu$ m predictions to the observed count rate, or 4:54  $\times 10^2$  M Jy sr $^{-1}$  (DN/s) $^{-1}$ , with a formal uncertainty of 0.7%. At the pixel scale of our mosaics, this factor is equivalent to 6:40  $\times 10^6$  Jy pixel $^{-1}$  (DN/s) $^{-1}$  (which can be converted to other pixel scales by multiplying by the square of the ratio of the pixel size to 2 $^0$ .45). Following Rieke et al. (2007), we assign an uncertainty of 2% to the calibration factor to allow for systematic effects in propagating the near-infrared measurements to 24  $\mu$ m. Where care is taken to apply the corrections discussed in x 2 and to treat calibration stars and other targets in a consistent manner, this calibration accuracy

can be maintained in science data. The data used to compute the calibration factor are summarized in Table 3.

The calibration factor was derived using stars, and no color corrections were applied to the measurements used here. Stars are relatively blue ( $f_{\lambda} / \lambda^2$ ) at MIPS wavelengths, so color corrections are required to calibrate sources with different spectral distributions. As shown by Stansberry et al. (2007), however, these corrections are small in the MIPS 24  $\mu$ m band: they are no more than 3% over a range of power-law indices (3 to 3) and do not exceed 5% for blackbody sources above a temperature of 57 K.

#### 4. SAMPLE AND PREDICTED FLUXES

The sample of stars used in  $\times 3$  to derive the 24  $\mu$ m calibration factor covers a limited dynamic range and is too small to probe statistically characteristics of the instrument behavior such as linearity and the effects of sky brightness. Furthermore, these stars are too faint to be useful as calibrators for the MIPS 70  $\mu$ m band (discussed by Gordon et al. 2007). In this section, we develop an expanded sample of 24  $\mu$ m calibrators to support our characterization of the performance of the instrument, which we discuss in  $\times 5$ . These stars were selected to explore the dynamic range of the instrument within reasonable integration times and to probe the effects of spectral type and environment (primarily foreground/background level) on the calibration.

##### 4.1. Zero-point Conversions for Additional Data Sets

We predict flux densities at 24  $\mu$ m for the expanded MIPS calibration target list by extrapolating measurements made at near- and mid-infrared wavelengths. The scale factors for the 2MASS (Skrutskie et al. 2006) measurements of A and G stars made in the read-1 (the 51 ms exposure used to measure sources that saturate the full 1.3 s exposure) data are given by Rieke et al. (2007), who find  $K_s [24]$  is 0 (by definition) and 0.045–0.011 magnitudes, respectively. The 2MASS read-1 magnitude limit ( $\sim 3.5$  magnitudes at  $K_s$ ) is not low enough to constrain measurements throughout the MIPS dynamic range, so we must incorporate additional data sets into our flux predictions for the bright 24  $\mu$ m calibrators. We discuss here the validation of additional data sets and derive the scale factors required to put them on the same system as the 2MASS read-1 measurements (and therefore the same system as the MIPS 24  $\mu$ m measurements), allowing direct comparison to the results of Rieke et al. (2007).

##### 4.1.1. 2MASS Saturated-Source Magnitudes

Below magnitudes of 4.5, 4, and 3.5 at J, H, and  $K_s$ , respectively, 2MASS data are saturated even in the read-1 measurements used to constrain the calibration factor derived in  $\times 3$ . Measurements for saturated sources are reported by the 2MASS project and are obtained by fitting to the radial profiles of the unsaturated portion of the stellar image, but large uncertainties (20%–30%) are associated with these measurements. To reduce the uncertainties associated with using the saturated 2MASS magnitudes, we compute the offset between the saturated and read-1 magnitudes.

Kinwenger (2005) presents photometry in the J and  $K_s$  bands for a sample of 600 stars that overlaps the 2MASS read-1 and saturated-source magnitude

ranges. This bright-star survey uses the same camera as the Deep Near-Infrared Survey of the Southern Sky (DENIS) with the addition of neutral-density filters, so we apply the DENIS transformations computed by Carpenter (2001) to put the magnitudes on the 2MASS system. (This step isn't strictly necessary since, as we discuss below, we are using these measurements differentially.) We compare the 2MASS measurements to those by Kinwenger (2005) over different magnitude ranges to determine the offset between the 2MASS read-1 and saturated-source magnitudes. At faint levels (well above the limits quoted above, to ensure that read-1 measurements were not affected by any saturated sources), the 2MASS and the transformed Kinwenger (2005) magnitudes are in excellent agreement: the weighted average (rejecting points more than 3  $\sigma$  from the median) of  $J(2MASS) - J(Kinwenger)$  between magnitudes 8.5 and 5.6 is 0.001–0.002 magnitudes, and  $K_s(2MASS) - K_s(Kinwenger)$  between magnitudes 7.5 and 4.2 is 0.023–0.003 magnitudes. Below those magnitude limits, the offsets are  $J(2MASS) - J(Kinwenger) = 0.053 - 0.005$  magnitudes and  $K_s(2MASS) - K_s(Kinwenger) = 0.058 - 0.008$  magnitudes. The difference between the faint J magnitudes is not significant, but we do include the difference between the faint  $K_s$  magnitudes in computing offsets ( $m_{read-1} - m_{saturated}$ ) of 0.053 magnitudes at J and 0.035 magnitudes at  $K_s$ . These offsets are added to saturated 2MASS magnitudes to put them on the read-1 scale. To further reduce the uncertainty, we average the J and  $K_s$  magnitudes to compute a "super- $K_s$ " magnitude, after correcting J to  $K_s$  using the J– $K$  colors (after correcting the colors to the 2MASS system using the transformations computed by Carpenter 2001) of stars tabulated by Tokunaga (2000).

##### 4.1.2. Johnson Photometry

Johnson et al. (1966) measured 650 bright stars in the J and K bands. This sample is large, homogeneously observed, and the measurements have significantly smaller uncertainties than the saturated sources observed by 2MASS. For example, the star HD 001013 was observed 91 times by Johnson et al. (1966). After applying an aimass correction derived from the data, we find a root-mean-square (RMS) deviation of 0.037 magnitudes in these measurements. We conservatively assign a 1  $\sigma$  uncertainty of 0.04 magnitudes to the photometry by Johnson et al. (1966).

To compute the offset between the Johnson et al. (1966) magnitudes and 2MASS, we transform the measurements to the 2MASS system using the equations derived by Carpenter (2001) for the Koornneef (1983) system, which is most similar to the system used by Johnson et al. (1966). The weighted average (rejecting points more than 3  $\sigma$  from the median) of  $J(2MASS) - J(\text{transformed Johnson})$  is 0.028–0.007 magnitudes and  $K_s(2MASS) - K_s(\text{transformed Johnson})$  is 0.004–0.005 magnitudes. The offset in the  $K_s$  band is not significant, but we apply a correction of 0.028 magnitudes to the measurements at J. In addition, since all the MIPS calibrators that were also measured by Johnson et al. (1966) are well into the saturated 2MASS range, we apply the same offsets applied to the saturated 2MASS measurements, for net corrections of 0.025 magnitudes

at J and 0.035 m magnitudes at  $K_s$  (plus the color transformation from Johnson to 2MASS). Finally, we combine the J and  $K_s$  data to form super- $K_s$  as for the 2MASS data.

#### 4.1.3. IRAS Measurements

Many of the bright MIPS calibrators were detected by IRAS at 12 and 25  $\mu$ m. The MIPS 24  $\mu$ m band was demonstrated by Rieke et al. (2007) to be linear within 1% below 1 Jy, so we can use the overlap between MIPS and IRAS measurements in this flux range to constrain the linearity of IRAS and probe for effects of molecular absorptions in the 12  $\mu$ m band. To ensure that the IRAS measurements are on the same scale as the other photometry we use to predict flux densities for our calibrators, we empirically derive the ratio between the IRAS bands and the MIPS 24  $\mu$ m band below 1 Jy for the calibrator stars, then apply this result over the full range of calibrator fluxes.

We obtain IRAS measurements of the MIPS calibrators from the faint source catalog (FSC; used because the improved sensitivity relative to the point source catalog provides more overlap with the MIPS sample), using only high-quality (quality flag \3") measurements. We applied color corrections appropriate to the temperature of each star to these observations and also applied the corrections measured by Rieke et al. (2007): 0.992 at 12  $\mu$ m and 0.980 at 25  $\mu$ m. The ratio of the MIPS 24  $\mu$ m measurement to the IRAS measurement, normalized to the average ratio, is plotted in Figure 5. The scatter in the measurements becomes obviously larger near the IRAS detection limit, around the equivalent 24  $\mu$ m flux density of 60 and 80 mJy at 12 and 25  $\mu$ m, respectively. The slope of the ratio as a function of brightness above these limits is consistent with 0 for both bands, indicating they are linear in this brightness range. The average value of  $f(24 \mu\text{m})=f(12 \mu\text{m})$  is 0.265 while  $f(24 \mu\text{m})=f(25 \mu\text{m})$  is 1.11. Both values are very similar to the values derived from Kunuz (1993) models of these stars, 0.266 and 1.11, respectively. As shown in Figure 6,  $f(24 \mu\text{m})=f(12 \mu\text{m})$  has a mild dependence on temperature (possibly the result of molecular absorptions in the 12  $\mu$ m band becoming important in cool stars), so the ratio is better described as  $0.276 \pm 1.94 \times 10^{-6} T_{\text{eff}} [\text{K}]$ . No significant trend with temperature is detected at 25  $\mu$ m.

The factors we derive in this section to convert the zero points of saturated 2MASS magnitudes, Johnson et al. (1966) magnitudes, and IRAS 12  $\mu$ m and 25  $\mu$ m measurements to the system used by MIPS are summarized in Table 4.

#### 4.2. The Calibration of Cool Stars

We compute an average super- $K_s$  [24] (by applying the aperture correction, 1.08, derived in x 2.4 and the calibration factor derived in x 3 to the measurements in Table 2) color for the cool (K and M giants) stars in our sample, which can be compared directly to the A and G star color computed by Rieke et al. (2007), modulo any offset (typically a fraction of a percent) between super- $K_s$  and  $K_s$ . The weighted average color of the K and M stars in our sample (after rejecting points greater than 3 from the mean) is 0.104  $\pm$  0.006 magnitudes.

#### 4.3. Predictions

We list the photometry used to constrain the flux density predictions, after applying the corrections detailed above, in Table 5. The 24  $\mu$ m flux densities for each source are the weighted average of the predictions derived from the entries in that table. We also list the predicted flux densities and their uncertainties in Table 5. We note that the predictions can be slightly different than those implicit in Table 3, since we used super- $K_s$  in Table 5 and  $K_s$  was used in Table 3, although the average difference is insignificant: 0.002  $\pm$  0.005 magnitudes. We also include predicted background levels, computed using the Spitzer Planning Observations Tool<sup>7</sup> (SPOT); the background listed is the average of the range when the target is visible, and the uncertainty is half the difference between the extreme values.

### 5. CHECKS ON THE 24 $\mu$ m CALIBRATION

In this section, we perform various checks on the 24  $\mu$ m calibration, such as repeatability, linearity, and the effects of spectral type, exposure time, and background. Except for the repeatability check, we compute a single calibration factor for each star by dividing the prediction (Table 5) by the pixel area and the weighted average of all measurements of the count rate for each star (Table 6). The calibration factors derived from some stars differ from the adopted calibration factor by more than 5%—these stars were not used in the checks below. As shown in Table 7, most of the rejected stars show infrared fluxes above the predictions (i.e., the calibration factor is low).

#### 5.1. Repeatability

The primary routine calibrator for the MIPS 24  $\mu$ m channel is HD 159330, a K2III star near the Spitzer continuous viewing zone (CVZ). When visible, this star is observed each time the instrument is turned on, to monitor photometric stability and check for changes in the calibration. A second routine calibrator, the K0III star HD 173398, is also monitored to fill in the gaps when HD 159330 is not visible. We plot 100 measurements of HD 159330 and 46 measurements of HD 173398 in Figure 7. The RMS scatter in the HD 159330 measurements is 0.4% (compared to 0.7% in the SSC-pipeline-reduced data discussed in x 2.5), while the scatter in the HD 173398 measurements is 0.5%. A gradual reduction in the instrument response of  $\sim$ 0.5% over the first 300 days is apparent in the data and is the cause of some of the scatter computed for HD 159330. As this trend is insignificant compared to the uncertainty on the absolute calibration (cf. x 3), we have not attempted to correct it.

#### 5.2. Linearity

We check for effects of flux nonlinearity in the calibration by comparing calibration factors over a range of 460 in source brightness. We plot the calibration factors in Figure 8. We find no significant trend of calibration factor with source brightness; a least-squares fit to the data shows a difference of only 0.3% between 9 mJy and 4 Jy. The observed scatter of calibration factors is larger than

<sup>7</sup> <http://ssc.spitzer.caltech.edu/proplot/spot/>

can be explained by the error bars. The unaccounted-for scatter in the calibration factors is likely due to systematic uncertainties on the flux predictions for the individual stars, possibly from variability or small infrared excesses.

### 5.3. Spectral Type

As discussed in x4, we have derived calibration factors using 3 broad types of stars (hot dwarfs, solar analogs, and coolgiants) to look for systematic effects with stellar temperature. The weighted average calibration factor of each broad spectral type is  $4.49 \times 10^{-2}$ ,  $4.62 \times 10^{-2}$ , and  $4.49 \times 10^{-2}$  M Jy/sr/ (DN/s) for 32 A, 37 G, and 25 K/M stars, respectively. These values are all consistent with the adopted calibration factor within the uncertainty (deviating by -1.1%, 1.8%, and -1.1%, respectively), but the differences may reflect real uncertainties in the colors of different types of stars and in our treatment of saturated 2M ASS magnitudes.

### 5.4. Exposure Time

A small subset of the calibrators (11 stars) was measured using 10- and 30-second exposures in addition to the 3-second exposures| the weighted average counts per second from these stars is 1% and 2% higher using 10- and 30-second exposures, respectively. We find that the residual images in the 10- and 30-second exposures are roughly twice as bright as in the 3-second exposures, so it is likely that the excess is due to buildup of residual charge during the longer exposures.

### 5.5. Background

In general, astronomical sources of interest at 24  $\mu$ m will be observed against a wide range of background levels, so we examine whether the derived calibration factor depends on background. Such an effect might be expected due to background light scattering onto the detector or due to systematic effects on the droop correction. We find no significant effect on the calibration over a factor of 5 in background, as shown in Figure 9. A least-squares fit to the data indicates a slope of only marginal significance:  $5.4 \times 10^{-4} \pm 2.9 \times 10^{-4}$  M Jy/sr/ (DN/s) / M Jy/sr.

### 5.6. Comparison to Another Infrared Calibration

As discussed in detail by Rieke et al. (2007) and cited in x4.1.3, the calibration presented here is based on an updated calibration system which is offset by a small ( $\pm 3\%$ ) amount from other infrared calibrations commonly in use. For the convenience of the reader, we present a direct comparison of our measurements to predictions in one of those systems, that prepared by Cohen and collaborators. Specifically, we compute predicted flux densities at 24  $\mu$ m for the 10 "template" stars (Cohen et al. 1999, and references therein) observed by us by interpolating the values given by the templates. We adopt the model uncertainties provided by the templates. We take the "observed" values and uncertainties from Table 6 and convert them to flux densities using the calibration factor computed in x3. We present the data used for and the results of this comparison in Table 8, where we reject the star HD 020722 due to a contaminating background source at 24  $\mu$ m (cf. Table 7). The

weighted average ratio of our measurements to the predictions is  $1.026 \pm 0.013$ , i.e., measurements on the Cohen et al. (1999) system can be converted to the system used by MIPS by multiplying by this factor. Much of this difference is due to the different fluxes adopted for Vega at 10.6  $\mu$ m ( $35.03$  Jy by Rieke et al. (2007) and  $34.38$  Jy by Cohen et al. (1999), which differ by 2%).

### 5.7. Extended-Source Calibration

As demonstrated in x2, the model PSF is a good match to the data out to large radii, so we expect the extrapolation of the calibration to infinite radii to be well understood. As a check, we compare measurements of extended sources (nearby galaxies) observed by the Spitzer legacy teams SINGS (Spitzer Infrared Nearby Galaxies Survey; Kennicutt et al. 2003) and SAGE (Surveying the Ages of a Galaxy's Evolution; Meixner et al. 2006) and by guaranteed time observers (Hinz et al. 2004; Gordon et al. 2006a,b) to IRAS measurements. We apply color corrections from Beichm an et al. (1988) (IRAS) and Stansberry et al. (2007) (MIPS) assuming a power-law spectrum fit to the 12/25  $\mu$ m or 24/70  $\mu$ m data to the IRAS and MIPS (SINGS measurements taken from Dale et al. 2007) measurements, and also correct the MIPS measurements to the calibration factor derived in x3. We interpolate the IRAS 12  $\mu$ m and 25  $\mu$ m measurements to the effective wavelength of the 24  $\mu$ m band, 23.675  $\mu$ m. We compare the results graphically in Figure 10. The weighted average ratio of MIPS to IRAS measurements is 0.96, well within the 8% combined uncertainty of both instruments.

## 6. SUMMARY

We discuss the flux calibration of the MIPS 24  $\mu$ m band, which is based on stars. We describe the data reduction and photometric procedures we use for the calibration sources, which produce fluxes that are  $1.6 \pm 0.6\%$  lower than those achieved by the automated pipeline at the Spitzer Science Center. We show that the calibration of the two imaging modes, photometry and scan map, is consistent within 1%.

We compute the calibration factor (the conversion from count rate to physical units) for the MIPS 24  $\mu$ m band, using a sample of 22 A stars that has been well measured and has been carefully vetted to exclude debris-disk systems. We find a value of  $4.54 \times 10^{-2}$  M Jy sr<sup>-1</sup> (DN/s)<sup>-1</sup>, with an uncertainty of 2%. Based on this uncertainty and the difference between the SSC pipeline and the DAT discussed in x2.5 and summarized above, we recommend that a net uncertainty on the calibration of 4% is appropriate for general use.

We present a sample of 238 stars appropriate for use as MIPS flux calibrators. We have computed flux densities of these stars at the effective wavelength of the 24  $\mu$ m band, 23.675  $\mu$ m. We present 348 measurements of 141 of these stars, and combine those measurements with the 24  $\mu$ m predictions to test various aspects of the calibration. We find that routine monitoring of a star near the Spitzer constant viewing zone demonstrates that 24  $\mu$ m photometry with MIPS is repeatable to 0.4%. The calibration is linear to 0.3% over a range of 460 in flux density, and there are no significant systematic effects on the calibration due to spectral type, background, or angular extent of the source.

We thank John Carpenter for helpful discussions, especially regarding the effect of exposure time on the measured count rate. We would also like to thank the anonymous referee, whose comments improved this paper. This work is based on observations made with the Spitzer Space Telescope, which is operated by the Jet Propulsion Laboratory, California Institute of Technology under NASA contract 1407. This research has made use of the SIMBAD database, operated at CDS,

Strasbourg, France. This publication makes use of data products from the Two Micron All Sky Survey, which is a joint project of the University of Massachusetts and the Infrared Processing and Analysis Center/California Institute of Technology, funded by the National Aeronautics and Space Administration and the National Science Foundation. Support for this work was provided by NASA through Contract Number # 1255094 issued by JPL/Caltech.

## REFERENCES

- Beichman, C. A., Neugebauer, G., Habing, H. J., Clegg, P. E., & Chester, T. J. 1988, *Infrared astronomical satellite (IRAS) catalogs and atlases. Volume 1: Explanatory supplement*
- Bloem aert, J. A. D. L., et al. *The ISO Handbook, Volume II - CAM - The ISO Camera*
- Bryden, G., et al. 2006, *ApJ*, 636, 1098
- Carpenter, J. M. 2001, *AJ*, 121, 2851
- Cohen, M., Walker, R. G., Carter, B., Ham m ersley, P., K idger, M., & Noguchi, K. 1999, *AJ*, 117, 1864
- Cohen, M., Walker, R. G., Jayaram an, S., Barker, E., & P rice, S. D. 2001, *AJ*, 121, 1180
- Dale, D. A., et al. 2007, *ApJ*, 655, 863
- Decin, L., Waelkens, C., Eriksson, K., Gustafsson, B., Plez, B., Sauval, A. J., Van Assche, W., & Vandenbussche, B. 2000, *A & A*, 364, 137
- Fadda, D., et al. 2006, *AJ*, 131, 2859
- Fazio, G. G., et al. 2004, *ApJS*, 154, 10
- Gordon, K. D., et al. 2005, *PASP*, 117, 503
- Gordon, K. D., et al. 2006a, *ApJ*, 638, L87
- Gordon, K. D., Engelbracht, C. W., Smith, J.-D. T., Rieke, G. H., & Misselt, K. A. 2006b, *astro-ph/0605544*
- Gordon, K. D., et al. 2007, submitted to *PASP*
- Gry, C., et al. *The ISO Handbook, Volume III - LWS - The Long Wavelength Spectrometer*
- Hauser, M. G., Kelsall, T., Leisawitz, D., & Weiland, J. 1998, *COBE Di use Infrared Background Experiment (DIRBE) Explanatory Supplement*
- Hinz, J. L., et al. 2004, *ApJS*, 154, 259
- Houck, J. R., et al. 2004, *ApJS*, 154, 18
- Johnson, H. L., Iriarte, B., Mitchell, R. I., & Wisniewski, W. Z. 1966, *Communications of the Lunar and Planetary Laboratory*, 4, 99
- Kennicutt, R. C., Jr., et al. 2003, *PASP*, 115, 928
- Kim eswenger, S. 2005, *High Resolution Infrared Spectroscopy in Astronomy*, 411
- Klaas, U., et al. 2003, *ESA SP-481: The Calibration Legacy of the ISO Mission*, 19
- Koomneef, J. 1983, *A & A*, 51, 489
- Krist, J. 2002, *Tiny Tim /SIRTF User's Guide (Pasadena: SSC)*
- M eixner, M., et al. 2006, *astro-ph/0606356*
- P rice, S. D., Paxson, C., Engelke, C., & M urdock, T. L. 2004, *AJ*, 128, 889
- Reach, W. T., et al. 2005, *PASP*, 117, 978
- Rieke, G. H., et al. 2004, *ApJS*, 154, 25
- Rieke, G. H., et al. 2005, *ApJ*, 620, 1010
- Rieke, G. H., et al. 2007, in preparation
- Schulz, B., et al. 2002, *A & A*, 381, 1110
- Skutskie, M. F., et al. 2006, *AJ*, 131, 1163
- Stansberry, J. A., et al. 2007, submitted to *PASP*
- Su, K. Y. L., et al. 2006, *ApJ*, in press
- Tokunaga, A. T. 2000, in *Allen's Astrophysical Quantities*, 4th edition, ed. A. N. Cox, Springer-Verlag: NY, p. 143
- W emer, M. W., et al. 2004, *ApJS*, 154, 1

TABLE 1  
 24 m Aperture Correction Factors for a 10,000 K Blackbody.<sup>a</sup>

description	radius	background annulus					
		6-8	7-13	20-32	40-50	none	
half 1st dark ring	3.5	2.78	2.80	2.57	2.56	2.56	
center of 1st dark ring	7.0		2.05	1.61	1.61	1.61	
outside 1st bright ring	13.0				1.17	1.16	1.16
center of second dark ring	20.0				1.15	1.13	1.12
outside second bright ring	35.0					<sup>b</sup> 1.0608	

<sup>a</sup>All radii are measured in arcseconds.

<sup>b</sup>Aperture correction used for calibration.



TABLE 2  
24 m Measurements of MIPS flux calibrators.

Name	days since mission start	AORKEY <sup>a</sup>	DCE <sup>b</sup> time (s)	count rate (DN/s)	uncertainty (DN/s)
BD + 621644	496.4	13071616	3	1.033e+04	5.19e+01
HD 000319	300.4	3972864	3	6.708e+03	5.00e+01
HD 001160	322.3	10090496	3	1.395e+03	1.56e+01
HD 001644	322.3	10090752	3	8.191e+03	5.69e+01
HD 002151	806.5	16276992	3	3.271e+05	1.23e+03
HD 002811	298.4	9940224	3	1.591e+03	3.35e+01
HD 008941	359.7	5414400	3	7.202e+03	3.46e+01
HD 009927	871.5	16619776	3	6.045e+05	2.45e+03
HD 011413	298.5	3973376	3	7.866e+03	3.87e+01
HD 014943	298.4	9940480	3	7.180e+03	2.84e+01
HD 015008	69.4	7345408	3	2.698e+04	1.14e+02
	84.0	7979264	3	2.662e+04	1.09e+02
	1133.7	20460800	3	2.672e+04	5.28e+01
	1133.6	20461056	30	2.730e+04	1.51e+01
	1133.7	20461312	10	2.705e+04	2.31e+01
HD 015646	394.6	3973888	3	2.997e+03	4.84e+01
HD 017254	339.7	11783424	3	4.482e+03	2.75e+01
	466.2	12871936	3	4.578e+03	2.81e+01
	1133.6	20462848	3	4.649e+03	5.28e+01
	1133.6	20463104	10	4.575e+03	2.31e+01
	1133.6	20463360	30	4.689e+03	1.44e+01
HD 019019	367.9	5407744	3	6.204e+03	3.74e+01
HD 020722	386.5	12063488	3	5.818e+03	4.56e+01
HD 020888	339.7	11783680	3	5.624e+03	2.99e+01
	630.9	13613568	3	5.427e+03	2.79e+01
HD 020902	905.8	16868864	3	6.872e+05	2.62e+03
HD 021981	153.6	8812544	10	6.089e+03	1.33e+01
HD 025860	702.7	15421440	3	4.202e+03	3.26e+01
HD 027466	392.1	5412096	3	3.146e+03	3.18e+01
HD 028099	762.9	15991808	3	2.546e+03	2.80e+01
HD 028471	181.1	9059072	10	3.173e+03	1.81e+01
HD 029461	762.9	15992064	3	2.759e+03	2.77e+01
HD 030246	762.9	15992320	3	2.497e+03	2.75e+01
HD 032831	386.4	12062464	3	2.301e+05	8.06e+02
HD 034868	179.9	3983360	3	3.851e+03	3.89e+01
HD 035666	364.2	11891968	3	3.416e+04	1.34e+02
HD 036167	920.0	16869120	3	5.627e+05	2.23e+03
HD 037962	414.8	5412864	3	3.281e+03	3.12e+01
HD 038949	416.4	5340160	3	2.871e+03	3.10e+01
HD 039608	61.0	7200768	3	3.844e+04	1.49e+02
	69.9	7743232	3	3.832e+04	1.46e+02
	84.0	7977472	3	3.805e+04	1.43e+02
	1133.7	20460032	3	3.780e+04	5.19e+01
	1133.7	20460288	10	3.842e+04	2.38e+01
	1133.7	20460544	30	3.878e+04	1.56e+01
HD 040129	386.5	12062720	3	2.025e+03	2.04e+01
HD 040335	202.7	9192192	3	2.866e+03	3.25e+01
HD 041371	386.5	12062976	3	1.491e+04	7.41e+01
	1133.7	20461568	10	1.494e+04	2.29e+01
	1133.7	20461824	30	1.502e+04	1.42e+01
	1133.7	20463616	3	1.462e+04	5.06e+01
HD 042525	631.5	13588224	3	5.116e+03	2.85e+01
HD 042701	35.3	6772992	3	4.363e+04	1.79e+02
	228.2	9457920	3	4.333e+04	1.61e+02
HD 043107	34.1	6765056	3	7.581e+03	1.05e+02
	34.1	6765312	10	7.757e+03	7.84e+01
	34.1	6765568	30	8.214e+03	7.31e+01
	34.1	6765824	3	8.087e+03	6.96e+01
	69.5	7342080	3	8.176e+03	6.96e+01
	69.5	7342336	10	8.386e+03	5.52e+01
	69.5	7344640	3	8.373e+03	1.64e+01
	69.5	7344896	3	8.104e+03	2.50e+01
	69.2	7346944	3	8.090e+03	6.99e+01
	69.3	7347200	3	7.298e+04	3.53e+02
	69.3	7347968	3	8.048e+03	6.92e+01
	91.8	7866112	3	8.122e+03	6.60e+01
	91.8	7866368	3	7.984e+04	4.24e+02
	91.8	7867136	3	8.206e+03	6.32e+01
HD 044594	70.6	7339008	3	9.411e+03	4.79e+01
HD 045557	631.5	13588480	3	5.492e+03	3.51e+01
HD 046190	258.0	9662976	3	3.703e+03	2.82e+01
HD 046819	393.7	12063232	3	8.504e+03	4.94e+01
HD 047332	364.2	11892224	3	2.595e+03	2.60e+01
HD 050310	205.7	9192448	3	7.865e+05	2.88e+03

TABLE 2 | Continued

Name	days since mission start	AORKEY <sup>a</sup>	DCE <sup>b</sup> time (s)	count rate (DN/s)	uncertainty (DN/s)
HD 053501	35.3	6773248		3 1.837e+ 05	6.89e+ 02
	60.9	7199232		3 1.840e+ 05	6.66e+ 02
	69.9	7742976		3 1.840e+ 05	7.02e+ 02
	84.0	7977728		3 1.831e+ 05	1.06e+ 03
HD 057336	631.5	13588736		3 1.403e+ 03	3.44e+ 01
HD 058142	49.7	7145472		3 1.458e+ 04	1.33e+ 02
HD 060178	228.2	9458176		3 2.584e+ 05	7.17e+ 02
HD 061929	631.5	13588992		3 3.038e+ 03	2.66e+ 01
HD 064324	416.9	5400832		3 3.672e+ 03	3.87e+ 01
HD 065517	631.6	13589248		3 2.122e+ 03	1.81e+ 01
HD 066751	416.2	5409280		3 9.671e+ 03	2.80e+ 01
HD 069863	631.5	13589504		3 1.240e+ 04	5.52e+ 01
HD 073210	226.2	3986432		3 3.707e+ 03	5.55e+ 01
HD 073666	227.7	3986688		3 2.541e+ 03	5.66e+ 01
HD 073819	226.2	3987200		3 3.170e+ 03	5.29e+ 01
HD 077281	627.2	13589760		3 1.673e+ 03	1.99e+ 01
HD 080007	319.4	10091008		3 2.592e+ 05	9.55e+ 02
	339.8	11783936		3 2.596e+ 05	9.23e+ 02
HD 082308	97.0	7973888		3 7.022e+ 05	2.59e+ 03
HD 082621	70.6	7338496		3 1.909e+ 04	8.24e+ 01
HD 087901	96.9	7972096		3 2.350e+ 05	7.87e+ 02
HD 091375	258.0	9663232		3 1.602e+ 04	6.73e+ 01
HD 092788	494.8	5440512		3 5.299e+ 03	3.93e+ 01
HD 092845	301.2	3990016		3 7.166e+ 03	4.51e+ 01
HD 096833	97.0	7974144		3 7.470e+ 05	2.80e+ 03
	869.7	16619008		3 7.373e+ 05	3.09e+ 03
HD 098230	869.7	16619264		3 1.467e+ 05	4.65e+ 02
HD 098553	301.2	5408512		3 3.858e+ 03	3.39e+ 01
HD 100167	463.9	5420544		3 5.036e+ 03	3.57e+ 01
HD 101452	664.8	15247104		3 1.910e+ 03	3.50e+ 01
HD 101472	518.8	5343232		3 3.834e+ 03	3.44e+ 01
HD 101959	301.2	5419008		3 5.822e+ 03	3.20e+ 01
HD 102647	302.5	9940736		3 2.372e+ 05	7.01e+ 02
	869.7	16618752		3 2.358e+ 05	7.39e+ 02
HD 102870	298.4	9940992		3 1.309e+ 05	5.02e+ 02
HD 105805	278.5	3991808		3 5.734e+ 03	5.10e+ 01
HD 106252	284.1	5442816		3 4.749e+ 03	3.73e+ 01
HD 106965	521.7	13201920		3 1.248e+ 03	1.87e+ 01
HD 108799	322.4	5338624		3 1.242e+ 04	4.16e+ 01
HD 108944	518.7	5334784		3 4.431e+ 03	3.10e+ 01
HD 109612	524.6	13111808		3 1.260e+ 04	6.56e+ 01
HD 109866	524.9	13112064		3 4.368e+ 03	2.77e+ 01
HD 110304	905.9	16869376		3 1.510e+ 05	5.70e+ 02
HD 112196	492.2	5278976		3 6.345e+ 03	3.41e+ 01
HD 115043	281.5	6599168		3 7.863e+ 03	3.29e+ 01
HD 115780	563.2	13380864		3 1.022e+ 04	1.25e+ 02
	563.3	13383680		3 1.064e+ 04	1.38e+ 02
HD 116706	279.6	3994624		3 6.188e+ 03	5.01e+ 01
HD 119545	551.8	13313024		3 1.360e+ 05	2.33e+ 03
HD 121370	905.8	16836608		3 3.132e+ 05	1.17e+ 03
HD 121504	340.5	5438208		3 4.016e+ 03	4.34e+ 01
HD 122652	302.0	5428224		3 5.100e+ 03	2.87e+ 01
HD 123123	905.9	16869632		3 6.343e+ 05	2.39e+ 03
HD 127665	181.2	9059328		3 6.687e+ 05	2.51e+ 03
HD 128998	671.5	15247360		3 4.824e+ 03	2.79e+ 01
HD 129655	705.6	15421696		3 2.577e+ 03	2.87e+ 01
HD 131986	551.8	13313280		3 7.721e+ 03	9.91e+ 01
HD 132417	551.7	13313536		3 5.041e+ 03	5.49e+ 01
HD 132439	551.7	13313792		3 5.055e+ 03	3.77e+ 01
HD 134493	202.1	9191936		3 2.956e+ 04	1.24e+ 02
HD 138265	96.9	7972352		3 1.447e+ 05	5.20e+ 02
	202.1	9191680		3 1.443e+ 05	7.25e+ 02
HD 139698	551.7	13314048		3 8.006e+ 03	1.99e+ 02
HD 141937	345.4	5442048		3 5.126e+ 03	3.82e+ 01
HD 144873	671.6	15247616		3 1.723e+ 03	1.96e+ 01
HD 150680	364.5	11892480		3 3.335e+ 05	1.33e+ 03
HD 150706	110.2	5386240		3 6.656e+ 03	3.12e+ 01
HD 152222	96.9	7971584		3 5.203e+ 04	3.13e+ 02
	1136.3	20459520		3 5.187e+ 04	4.66e+ 01
	1136.3	20459776	10	5.142e+ 04	2.11e+ 01
HD 153458	387.1	5416704		3 2.799e+ 03	3.91e+ 01
HD 154391	96.9	7970560		3 3.023e+ 04	1.22e+ 02
HD 158460	96.9	7970048		3 7.931e+ 03	5.71e+ 01
HD 158485	96.9	7969280		3 3.564e+ 03	2.80e+ 01
HD 159048	96.9	7970816		3 3.600e+ 04	1.88e+ 02

TABLE 2 | Continued

Name	days since mission start	AORKEY <sup>a</sup>	DCE <sup>b</sup> time (s)	count rate (DN/s)	uncertainty (DN/s)
HD 159222	320.9	5436672	3	9.997e+03	2.90e+01
	634.1	13590016	3	9.787e+03	5.20e+01
	1134.3	20462080	3	1.019e+04	4.86e+01
	1134.3	20462336	10	9.952e+03	2.10e+01
	1134.3	20462592	30	1.020e+04	1.36e+01
HD 159330	42.5	6941696	3	7.978e+04	2.77e+02
	49.5	7143424	3	7.977e+04	3.18e+02
	49.5	7143680	3	7.957e+04	3.26e+02
	49.6	7143936	3	7.953e+04	3.27e+02
	49.6	7144192	3	7.934e+04	3.20e+02
	49.6	7144448	3	7.936e+04	3.06e+02
	53.8	7166976	3	8.024e+04	2.92e+02
	60.9	7200512	3	7.975e+04	2.96e+02
	61.4	7202048	3	8.030e+04	2.86e+02
	70.7	7337728	3	7.946e+04	2.95e+02
	69.4	7346688	3	7.951e+04	4.85e+02
	69.0	7348736	3	7.933e+04	2.79e+02
	73.4	7428608	3	7.980e+04	2.98e+02
	73.4	7430144	10	8.084e+04	3.96e+02
	58.8	7640320	3	7.979e+04	2.96e+02
	69.8	7744256	3	7.967e+04	2.97e+02
	90.6	7795712	3	7.915e+04	2.96e+02
	96.5	7974400	3	7.913e+04	2.87e+02
	84.1	7978752	3	7.963e+04	2.96e+02
	84.1	7980544	3	7.959e+04	2.94e+02
	104.8	8137216	3	7.927e+04	2.90e+02
	106.8	8137984	3	7.995e+04	3.03e+02
	107.9	8342016	3	7.977e+04	2.96e+02
	125.8	8379904	3	7.914e+04	2.91e+02
	127.2	8380672	3	7.958e+04	2.82e+02
	109.9	8782592	3	7.947e+04	2.84e+02
	153.5	8809472	3	7.964e+04	3.04e+02
	157.0	8819200	3	7.977e+04	2.99e+02
	162.1	8937472	3	7.979e+04	2.90e+02
	178.8	9066496	3	7.905e+04	2.90e+02
	182.2	9066752	3	7.926e+04	2.98e+02
	185.1	9181440	3	7.952e+04	3.00e+02
	201.7	9190912	3	7.900e+04	2.88e+02
	205.6	9221632	3	7.964e+04	3.01e+02
	209.5	9222400	3	7.960e+04	3.10e+02
	224.7	9457408	3	7.913e+04	3.00e+02
	231.9	9617664	3	7.928e+04	3.09e+02
	228.9	9640192	3	7.915e+04	3.16e+02
	250.7	9658368	3	7.918e+04	3.11e+02
	253.5	9658880	3	7.932e+04	3.02e+02
	258.0	9659392	3	7.937e+04	3.02e+02
	276.9	9802496	3	7.919e+04	3.11e+02
	281.7	9803264	3	7.919e+04	3.03e+02
	284.5	9804032	3	7.939e+04	3.17e+02
	298.2	9937152	3	7.898e+04	3.08e+02
	300.6	9938688	3	7.924e+04	3.19e+02
	303.5	9939456	3	7.910e+04	3.11e+02
	317.6	10087936	3	7.891e+04	2.99e+02
	319.7	10088704	3	7.931e+04	3.21e+02
	322.5	10089472	3	7.911e+04	3.08e+02
	338.6	11780352	3	7.878e+04	2.98e+02
	342.1	11781120	3	7.929e+04	3.11e+02
	345.1	11781888	3	7.969e+04	3.04e+02
	347.4	11782656	3	7.914e+04	2.95e+02
	359.7	11891200	3	7.911e+04	3.04e+02
	362.6	11897088	3	7.930e+04	3.11e+02
	368.0	11897856	3	7.930e+04	3.04e+02
	385.6	12060160	3	7.883e+04	2.99e+02
	389.5	12060928	3	7.921e+04	3.07e+02
	393.0	12061696	3	7.947e+04	2.98e+02
	397.8	12152832	3	7.941e+04	3.00e+02
	414.5	12194560	3	7.885e+04	2.85e+02
	418.0	12195328	3	7.875e+04	3.06e+02
	421.5	12196096	3	7.921e+04	2.99e+02
	438.8	12394496	3	7.934e+04	2.96e+02
	434.5	12395264	3	7.917e+04	2.96e+02
	443.4	12396032	3	7.952e+04	3.02e+02
	516.6	13108992	3	7.879e+04	2.88e+02
	529.4	13110016	3	7.901e+04	2.99e+02
	521.7	13111040	3	7.887e+04	3.04e+02

TABLE 2 | Continued

Name	days since mission start	AORKEY <sup>a</sup>	DCE <sup>b</sup> time (s)	count rate (DN/s)	uncertainty (DN/s)
	550.6	13295360	3	7.862e+04	2.90e+02
	557.8	13298176	3	7.933e+04	3.03e+02
	563.1	13299200	3	7.904e+04	3.02e+02
	584.5	13428992	3	7.880e+04	2.96e+02
	591.0	13431552	3	7.863e+04	2.97e+02
	596.6	13432320	3	7.905e+04	3.13e+02
	634.3	13585408	3	7.937e+04	3.14e+02
	624.6	13586176	3	7.866e+04	2.98e+02
	629.4	13586944	3	7.908e+04	3.02e+02
	634.4	13587712	3	7.944e+04	3.08e+02
	660.6	15217152	3	7.896e+04	3.01e+02
	667.8	15220480	3	7.917e+04	3.14e+02
	701.5	15413248	3	7.889e+04	3.00e+02
	704.9	15414272	3	7.898e+04	3.10e+02
	709.3	15415296	3	7.920e+04	3.09e+02
	731.6	15815168	3	7.899e+04	2.98e+02
	735.9	15816192	3	7.927e+04	3.04e+02
	742.1	15817216	3	7.919e+04	3.03e+02
	760.4	15991040	3	7.854e+04	3.04e+02
	767.9	16047616	3	7.916e+04	3.06e+02
	775.9	16048640	3	7.901e+04	2.95e+02
	800.4	16228608	3	7.868e+04	2.89e+02
	805.8	16254208	3	7.924e+04	3.00e+02
	810.8	16255232	3	7.925e+04	2.92e+02
	869.6	16603648	3	7.914e+04	2.92e+02
	872.1	16604416	3	7.909e+04	3.01e+02
	869.6	16619520	3	7.898e+04	2.96e+02
	904.0	16833792	3	7.899e+04	2.95e+02
	910.8	16834816	3	7.905e+04	2.91e+02
	921.2	16835840	3	7.883e+04	2.98e+02
	1134.3	20459008	3	7.921e+04	4.95e+01
	1134.3	20459264	10	7.932e+04	2.15e+01
HD 163466	96.9	7969024	3	2.952e+03	2.48e+01
	465.5	12872448	3	2.963e+03	3.71e+01
	630.4	13613824	3	2.841e+03	4.81e+01
HD 163588	97.0	7973376	3	4.503e+05	1.62e+03
	298.5	9942528	3	4.427e+05	2.42e+03
HD 165459	96.9	7968256	3	3.830e+03	3.82e+01
	283.0	9851392	3	3.853e+03	3.26e+01
HD 166780	96.9	7970304	3	3.072e+04	1.20e+02
	254.7	9660416	3	3.057e+04	1.30e+02
HD 167389	303.3	5434368	3	4.449e+03	2.66e+01
HD 170693	96.9	7971840	3	1.905e+05	6.87e+02
	905.8	16869888	3	1.877e+05	6.81e+02
	1136.3	20458496	3	1.830e+05	4.73e+01
	1136.3	20458752	10	1.861e+05	2.40e+01
HD 172066	96.9	7968512	3	3.368e+03	2.68e+01
HD 172728	96.9	7969792	3	4.754e+03	3.21e+01
	465.5	12872704	3	4.741e+03	3.04e+01
HD 173398	461.6	12871424	3	3.019e+04	1.21e+02
	466.6	12884224	3	3.050e+04	1.22e+02
	470.4	12884736	3	3.048e+04	1.26e+02
	484.6	12997120	3	3.014e+04	1.20e+02
	488.8	13001472	3	3.041e+04	1.24e+02
	496.4	13071872	10	3.082e+04	1.52e+02
	496.4	13072128	30	3.120e+04	1.52e+02
	496.5	13072640	3	3.030e+04	1.16e+02
	516.6	13108736	3	3.014e+04	1.15e+02
	529.4	13109760	3	3.016e+04	1.21e+02
	521.8	13110784	3	3.033e+04	1.23e+02
	550.5	13295104	3	3.013e+04	1.18e+02
	557.8	13297920	3	3.028e+04	1.22e+02
	563.0	13298944	3	3.020e+04	1.25e+02
	584.5	13428736	3	3.018e+04	1.22e+02
	591.0	13431296	3	3.016e+04	1.26e+02
	596.6	13432064	3	3.048e+04	1.32e+02
	634.3	13585152	3	3.043e+04	1.27e+02
	624.6	13585920	3	3.018e+04	1.24e+02
	629.4	13586688	3	3.026e+04	1.23e+02
	634.4	13587456	3	3.035e+04	1.28e+02
	660.6	15216896	3	3.006e+04	1.24e+02
	667.8	15220224	3	3.036e+04	1.26e+02
	674.2	15221248	3	3.043e+04	1.29e+02
	701.5	15412992	3	3.022e+04	1.23e+02
	704.9	15414016	3	3.036e+04	1.25e+02

TABLE 2 | Continued

Name	days since mission start	AORKEY <sup>a</sup>	DCE <sup>b</sup> time (s)	count rate (DN/s)	uncertainty (DN/s)
	709.3	15415040		3 3.047e+ 04	1.29e+ 02
	731.6	15814912		3 3.030e+ 04	1.21e+ 02
	735.9	15815936		3 3.031e+ 04	1.26e+ 02
	742.1	15816960		3 3.040e+ 04	1.28e+ 02
	760.4	15990784		3 3.000e+ 04	1.21e+ 02
	767.9	16047360		3 3.034e+ 04	1.27e+ 02
	775.9	16048384		3 3.023e+ 04	1.25e+ 02
	800.4	16228352		3 3.009e+ 04	1.22e+ 02
	805.8	16253952		3 3.076e+ 04	1.28e+ 02
	810.8	16254976		3 3.035e+ 04	1.19e+ 02
	827.8	16374528		3 3.000e+ 04	1.17e+ 02
	830.8	16375296		3 3.030e+ 04	1.22e+ 02
	835.9	16376832		3 3.031e+ 04	1.21e+ 02
	864.7	16602624		3 3.008e+ 04	1.18e+ 02
	869.6	16603392		3 3.043e+ 04	1.19e+ 02
	872.0	16604160		3 3.045e+ 04	1.23e+ 02
	904.0	16833536		3 3.037e+ 04	1.20e+ 02
	910.8	16834560		3 3.030e+ 04	2.03e+ 02
	921.2	16835584		3 3.040e+ 04	1.25e+ 02
	905.8	16870144		3 3.025e+ 04	1.28e+ 02
HD 173511	96.9	7971072		3 3.165e+ 04	1.24e+ 02
HD 173976	96.9	7971328		3 4.749e+ 04	1.72e+ 02
HD 174123	96.9	7968000		3 2.296e+ 03	2.39e+ 01
HD 176841	96.9	7968768		3 3.644e+ 03	2.79e+ 01
HD 180711	97.0	7973632		3 5.796e+ 05	2.09e+ 03
	280.7	9805568		3 5.722e+ 05	2.07e+ 03
HD 183439	70.7	7334144		3 7.201e+ 05	3.67e+ 03
	70.8	7335424		3 7.198e+ 05	3.81e+ 03
HD 189276	97.0	7973120		3 3.868e+ 05	1.38e+ 03
	280.7	9805824		3 3.844e+ 05	1.51e+ 03
HD 191854	96.9	7969536		3 5.075e+ 03	4.82e+ 01
	254.7	9660672		3 4.652e+ 03	3.60e+ 01
	254.7	9661184	10	4.922e+ 03	2.69e+ 01
HD 193017	415.0	5410560		3 4.150e+ 03	3.86e+ 01
HD 195034	439.3	5426688		3 6.127e+ 03	3.33e+ 01
HD 199598	301.8	5413632		3 7.021e+ 03	3.60e+ 01
HD 201941	280.7	9806080		3 2.900e+ 03	2.79e+ 01
HD 204277	435.3	5374976		3 7.301e+ 03	2.83e+ 01
HD 205905	417.6	5405440		3 7.871e+ 03	3.42e+ 01
HD 209952	69.4	7345152		3 1.468e+ 05	5.43e+ 02
	84.0	7979008		3 1.462e+ 05	5.16e+ 02
HD 212291	441.9	5421312		3 3.319e+ 03	3.19e+ 01
HD 216131	96.9	7972608		3 3.277e+ 05	1.24e+ 03
HD 216275	318.5	5435136		3 5.062e+ 03	4.07e+ 01
HD 217382	97.0	7972864		3 3.264e+ 05	1.18e+ 03
NPM 1+ 61.0569	465.5	12872960		3 1.510e+ 03	1.64e+ 01
NPM 1+ 68.0412	415.5	12196864		3 1.494e+ 03	1.67e+ 01
SAO 9310	415.5	12197120		3 1.069e+ 03	1.24e+ 01

<sup>a</sup> The "AORKEY," or Astronomical Observation Request Key, is used by the Spitzer Science Center to uniquely identify the observation.<sup>b</sup> "DCE" refers to "Data Collection Event," in this case an individual image.

TABLE 3  
Data Used to Compute the 24 m Calibration Factor

Name	$K_s^a$ (mag.)	24 m count rate (DN/s)	uncertainty (DN/s)	calibration factor ( $M \text{ Jy/sr/ DN/s}$ )	uncertainty ( $M \text{ Jy/sr/ DN/s}$ )
HD 000319	5.479	6.708e+ 03	5.00e+ 01	4.513e 02	1.39e 03
HD 002811	7.057	1.591e+ 03	3.35e+ 01	4.448e 02	1.63e 03
HD 011413	5.422	7.866e+ 03	3.87e+ 01	4.056e 02	1.23e 03
HD 014943	5.439	7.180e+ 03	2.84e+ 01	4.374e 02	1.32e 03
HD 015646	6.411	2.997e+ 03	4.85e+ 01	4.281e 02	1.46e 03
HD 017254	5.877	4.529e+ 03	1.97e+ 01	4.632e 02	1.40e 03
HD 020888	5.691	5.519e+ 03	2.04e+ 01	4.512e 02	1.36e 03
HD 021981	5.526	6.089e+ 03	1.33e+ 01	4.761e 02	1.43e 03
HD 034868	6.024	3.851e+ 03	3.89e+ 01	4.758e 02	1.51e 03
HD 042525	5.751	5.116e+ 03	2.85e+ 01	4.606e 02	1.40e 03
HD 057336	7.114	1.403e+ 03	3.44e+ 01	4.786e 02	1.86e 03
HD 073210	6.165	3.707e+ 03	5.55e+ 01	4.341e 02	1.45e 03
HD 073666	6.532	2.541e+ 03	5.66e+ 01	4.517e 02	1.69e 03
HD 073819	6.280	3.170e+ 03	5.29e+ 01	4.566e 02	1.57e 03
HD 092845	5.513	7.166e+ 03	4.51e+ 01	4.094e 02	1.26e 03
HD 101452	6.819	1.910e+ 03	3.50e+ 01	4.613e 02	1.62e 03
HD 105805	5.600	5.734e+ 03	5.10e+ 01	4.722e 02	1.48e 03
HD 116706	5.502	6.188e+ 03	5.01e+ 01	4.789e 02	1.49e 03
HD 128998	5.756	4.824e+ 03	2.79e+ 01	4.862e 02	1.48e 03
HD 158485	6.145	3.564e+ 03	2.79e+ 01	4.599e 02	1.43e 03
HD 163466	6.339	2.917e+ 03	2.94e+ 01	4.699e 02	1.49e 03
HD 172728	5.753	4.747e+ 03	2.21e+ 01	4.954e 02	1.50e 03

Note. | The average calibration factor is  $4.54 \cdot 10^{-2} M \text{ Jy sr}^{-1} (\text{DN/s})^{-1}$ , to which we've assigned an uncertainty of 2% (see x 3).

<sup>a</sup> $K_s = [24]$  for the stars in this table (see Reike et al. 2007), all of which are between types A 0 and A 6.

TABLE 4  
Zero-point Conversions

Data Set	Conversion Factor
2MASS saturated J	0.053 mag.
2MASS saturated K <sub>s</sub>	0.035 mag.
Johnson J	0.025 mag.
Johnson K	0.035 mag.
IRAS 12 $\mu$ m	0.266
IRAS 25 $\mu$ m	1:1

Note. | These factors convert measurements to 24  $\mu$ m magnitudes (NIR) or fluxes (IRAS) (see x 4.1).





## M IPS 24 m Calibration

17

TABLE 5 | Continued

Name	Spectral Type	super-K <sub>s</sub> <sup>a</sup> (m ag.)	unc. (m ag.)	f (12 m) <sup>b</sup> (Jy)	unc. (Jy)	f (25 m) <sup>b</sup> (Jy)	unc. (Jy)	predictions			
								f (24 m) <sup>c</sup> (Jy)	unc. (Jy)	bkgd <sub>24</sub> <sup>d</sup> (M Jy/sr)	unc. (M Jy/sr)
HD 056413	G 5V	7.307	0.016					8.927e 03	2.66e 04	1.57e+ 01	2.65e+ 00
HD 056855	K 3Ib	1.005	0.028	9.475e+ 01	3.79e+ 00	2.341e+ 01	9.37e 01	2.251e+ 01	5.16e 01	1.80e+ 01	3.34e+ 00
HD 057336	A 0IV	7.194	0.020					9.504e 03	2.83e 04	1.65e+ 01	2.72e+ 00
HD 057507	G 5V	7.114	0.018					1.066e 02	3.29e 04	1.56e+ 01	2.68e+ 00
HD 058142	A 1V	4.608	0.117	3.832e 01	2.30e 02			1.041e 01	5.62e 03	2.95e+ 01	6.98e+ 00
HD 059717	K 5III	0.468	0.028	4.924e+ 01	2.46e+ 00	1.199e+ 01	5.99e 01	1.258e+ 01	3.21e 01	1.74e+ 01	2.83e+ 00
HD 060178	A 2V	1.431	0.028	7.211e+ 00	4.33e 01	1.624e+ 00	8.12e 02	1.893e+ 00	5.01e 02	4.50e+ 01	1.22e+ 01
HD 060522	M 0III	0.202	0.028	2.549e+ 01	1.27e+ 00	5.944e+ 00	2.38e 01	6.593e+ 00	1.59e 01	4.91e+ 01	1.33e+ 01
HD 061929	G 5V	6.366	0.014	7.234e 02	1.09e 02			2.115e 02	5.97e 04	1.55e+ 01	2.56e+ 00
HD 062509	K 0IIIb	1.185	0.028	8.784e+ 01	3.51e+ 00	2.024e+ 01	1.01e+ 00	2.315e+ 01	5.54e 01	4.81e+ 01	1.30e+ 01
HD 064324	G 0	6.242	0.013					2.381e 02	6.73e 04	4.16e+ 01	1.10e+ 01
HD 065517	A 2/3IV	6.879	0.019					1.270e 02	3.70e 04	1.66e+ 01	2.79e+ 00
HD 066751	F 8	5.071	0.015	2.435e 01	1.95e 02			6.932e 02	1.91e 03	2.00e+ 01	3.84e+ 00
HD 069863	A 2V	4.954	0.014	3.275e 01	1.31e 02	7.684e 02	8.45e 03	7.822e 02	1.69e 03	1.55e+ 01	2.46e+ 00
HD 070272	K 4.5III	0.567	0.028	1.923e+ 01	9.62e 01	4.546e+ 00	2.27e 01	4.846e+ 00	1.24e 01	3.25e+ 01	7.63e+ 00
HD 071129	K 3III+	1.696	0.119	1.723e+ 02	5.17e+ 00	4.329e+ 01	1.73e+ 00	4.563e+ 01	1.12e+ 00	1.58e+ 01	2.57e+ 00
HD 073210	A 5V	6.185	0.015					2.407e 02	6.42e 04	4.96e+ 01	1.31e+ 01
HD 073666	A 1V	6.516	0.015					1.775e 02	4.73e 04	4.95e+ 01	1.28e+ 01
HD 073819	A 6V	6.283	0.014					2.199e 02	5.74e 04	4.95e+ 01	1.29e+ 01
HD 075223	A 1V	7.279	0.026					8.789e 03	3.00e 04	2.00e+ 01	3.53e+ 00
HD 077281	A 2	7.021	0.016					1.115e 02	3.03e 04	3.44e+ 01	9.28e+ 00
HD 080007	A 2IV	1.440	0.199	6.683e+ 00	2.67e 01	1.589e+ 00	6.36e 02	1.793e+ 00	5.22e 02	1.56e+ 01	2.61e+ 00
HD 080493	K 7III	0.667	0.028	5.859e+ 01	2.93e+ 00	1.376e+ 01	8.26e 01	1.490e+ 01	3.94e 01	3.74e+ 01	8.71e+ 00
HD 081797	K 3II-III	1.236	0.028	1.077e+ 02	6.46e+ 00	2.368e+ 01	1.42e+ 00	2.556e+ 01	7.06e 01	3.03e+ 01	7.64e+ 00
HD 082308	K 5III	0.567	0.028	2.031e+ 01	1.83e+ 00	4.486e+ 00	2.69e 01	4.798e+ 00	1.41e 01	4.76e+ 01	1.21e+ 01
HD 082621	A 2V	4.454	0.102	5.327e 01	3.20e 02			1.361e 01	7.16e 03	2.49e+ 01	4.74e+ 00
HD 082668	K 5III	0.507	0.140					1.259e+ 01	1.78e+ 00	1.85e+ 01	2.60e+ 00
HD 087901	B 7	1.508	0.028	6.272e+ 00	3.14e 01	1.466e+ 00	1.47e 01	1.765e+ 00	4.94e 02	4.97e+ 01	1.36e+ 01
HD 089388	K 3IIa	0.091	0.227					7.256e+ 00	1.66e+ 00	1.71e+ 01	2.68e+ 00
HD 089484	K 1IIIb	0.705	0.028	6.156e+ 01	2.46e+ 00	1.378e+ 01	5.51e 01	1.547e+ 01	3.52e 01	4.68e+ 01	1.14e+ 01
HD 089758	M 0III	0.967	0.028	7.416e+ 01	3.71e+ 00	1.775e+ 01	1.06e+ 00	1.936e+ 01	5.11e 01	2.85e+ 01	5.26e+ 00
HD 091056	M 0III	0.748	0.216					3.962e+ 00	8.60e 01	1.69e+ 01	2.77e+ 00
HD 091375	A 1V	4.696	0.320	4.151e 01	2.08e 02	1.081e 01	1.40e 02	1.134e 01	5.31e 03	1.62e+ 01	2.86e+ 00
HD 092305	M 0III	0.330	0.193	2.491e+ 01	9.97e 01	6.116e+ 00	3.06e 01	6.592e+ 00	2.09e 01	1.69e+ 01	2.95e+ 00
HD 092788	G 5	5.733	0.023					3.805e 02	1.29e 03	4.22e+ 01	1.17e+ 01
HD 092845	A 0V	5.548	0.015	1.815e 01	3.08e 02			4.340e 02	1.14e 03	2.17e+ 01	4.09e+ 00
HD 093813	K 0/K 1III	0.285	0.028	2.491e+ 01	1.49e+ 00	5.712e+ 00	4.00e 01	6.207e+ 00	1.76e 01	3.02e+ 01	6.93e+ 00
HD 095418	A 1V	2.248	0.028	3.320e+ 00	1.33e 01	9.755e 01	4.88e 02	9.326e 01	2.23e 02	2.12e+ 01	3.07e+ 00
HD 095578	M 0III	0.769	0.028	1.573e+ 01	1.10e+ 00	3.776e+ 00	2.27e 01	3.979e+ 00	1.13e 01	4.38e+ 01	1.22e+ 01
HD 095689	K 0Iab	0.663	0.028	5.893e+ 01	2.36e+ 00	1.389e+ 01	6.94e 01	1.502e+ 01	3.59e 01	1.99e+ 01	2.80e+ 00
HD 096833	K 1III	0.389	0.028	2.111e+ 01	1.06e+ 00	5.086e+ 00	2.54e 01	5.556e+ 00	1.42e 01	2.49e+ 01	3.80e+ 00
HD 098230	F 8.5V	2.095	0.187	4.067e+ 00	2.03e 01	8.777e 01	5.27e 02	1.036e+ 00	3.98e 02	3.15e+ 01	5.38e+ 00
HD 098262	K 3III	0.269	0.028	2.457e+ 01	1.23e+ 00	5.808e+ 00	2.90e 01	6.296e+ 00	1.60e 01	3.05e+ 01	5.07e+ 00
HD 098553	G 2.5V	6.080	0.015	1.239e 01	1.61e 02			2.782e 02	7.94e 04	2.99e+ 01	6.51e+ 00
HD 100029	M 0III	0.207	0.028	3.827e+ 01	1.53e+ 00	9.702e+ 00	4.85e 01	9.927e+ 00	2.38e 01	1.81e+ 01	2.53e+ 00
HD 100167	F 8	5.822	0.016	1.424e 01	1.71e 02			3.520e 02	1.02e 03	2.53e+ 01	3.60e+ 00
HD 101452	A 2	6.897	0.018					1.249e 02	3.55e 04	2.17e+ 01	3.49e+ 00
HD 101472	G 0	6.130	0.017	1.148e 01	1.95e 02			2.649e 02	7.91e 04	4.17e+ 01	1.10e+ 01
HD 101959	G 0V	5.617	0.015	1.486e 01	1.93e 02			4.218e 02	1.20e 03	2.55e+ 01	4.66e+ 00
HD 102647	A 3V	1.894	0.028	4.852e+ 00	2.91e 01			1.268e+ 00	3.90e 02	4.30e+ 01	9.18e+ 00
HD 102870	F 9V	2.226	0.179	3.622e+ 00	2.54e 01			9.641e 01	6.34e 02	5.00e+ 01	1.38e+ 01
HD 105707	K 2III	0.071	0.028	3.017e+ 01	1.81e+ 00	7.014e+ 00	4.21e 01	7.568e+ 00	2.09e 01	3.15e+ 01	6.42e+ 00
HD 105805	A 4V	5.607	0.022					4.099e 02	1.28e 03	3.05e+ 01	4.32e+ 00
HD 106252	G 0V	5.947	0.018	1.240e 01	1.86e 02			3.130e 02	9.47e 04	4.43e+ 01	9.84e+ 00
HD 106965	A 2	7.300	0.017					8.620e 03	2.40e 04	4.96e+ 01	1.31e+ 01
HD 108799	G 1.5V	4.864	0.016	3.295e 01	2.97e 02			8.498e 02	2.40e 03	4.19e+ 01	1.05e+ 01
HD 108903	M 3.5III	3.196	0.098					1.498e+ 02	1.51e+ 01	2.05e+ 01	3.56e+ 00
HD 108944	F 8	5.997	0.012	1.408e 01	2.11e 02			3.000e 02	8.21e 04	2.68e+ 01	3.13e+ 00
HD 109612	K 1/K 2III	5.067	0.014					7.419e 02	1.95e 03	2.50e+ 01	3.53e+ 00
HD 109866	K 0III	5.264	0.016					6.188e 02	1.70e 03	2.79e+ 01	3.55e+ 00
HD 110304	A 1IV	2.052	0.028	3.962e+ 00	1.98e 01	9.505e 01	4.75e 02	1.075e+ 00	2.73e 02	2.12e+ 01	3.93e+ 00
HD 112196	F 8V	5.553	0.017	1.769e 01	1.95e 02			4.505e 02	1.32e 03	3.02e+ 01	3.86e+ 00
HD 115043	G 1V	5.334	0.014	1.706e 01	1.71e 02			5.392e 02	1.49e 03	1.81e+ 01	1.51e+ 00
HD 115780	G 8/K 0III	6.237	0.016					2.525e 02	6.93e 04	3.54e+ 01	3.83e+ 00
HD 116706	A 3IV	5.489	0.015	1.670e 01	2.50e 02			4.569e 02	1.20e 03	2.69e+ 01	2.89e+ 00
HD 119545	K 1III	6.077	0.013					2.926e 02	7.55e 04	6.54e+ 01	4.01e+ 00
HD 120477	K 5.5III	0.317	0.028	2.360e+ 01	1.42e+ 00	5.362e+ 00	3.22e 01	5.961e+ 00	1.64e 01	3.03e+ 01	4.43e+ 00
HD 120933	K 5III	0.150	0.028	3.300e+ 01	1.98e+ 00	7.983e+ 00	5.59e 01	7.377e+ 00	2.10e 01	2.15e+ 01	1.40e+ 00
HD 121370	G 0IV	1.272	0.028	9.781e+ 00	1.56e+ 00			2.328e+ 00	8.52e 02	2.83e+ 01	3.81e+ 00
HD 121504	G 2V	6.167	0.047					2.551e 02	1.36e 03	2.22e+ 01	4.45e+ 00
HD 122652	F 8	5.855	0.015	1.293e 01	1.94e 02			3.402e 02	9.76e 04	2.20e+ 01	1.74e+ 00
HD 123123	K 2III	0.634	0.028	1.644e+ 01	8.22e 01	3.837e+ 00	2.30e 01	4.352e+ 00	1.15e 01	3.90e+ 01	9.60e+ 00
HD 123139	K 0IIIb	0.285	0.149	4.074e+ 01	2.04e+ 00	9.471e+ 00	5.68e 01	1.062e+ 01	4.03e 01	3.09e+ 01	7.05e+ 00
HD 124897	K 1.5III	2.951	0.116	5.324e+ 02	4.79e+ 01	1.117e+ 02	7.82e+ 00	1.273e+ 02	6.46e+ 00	2.68e+ 01	3.57e+ 00

TABLE 5 | Continued

Name	Spectral Type	super-K <sub>s</sub> <sup>a</sup> (mag.)	unc. (mag.)	f (12 m) <sup>b</sup> (Jy)	unc. (Jy)	f (25 m) <sup>b</sup> (Jy)	unc. (Jy)	predictions			
								f (24 m) <sup>c</sup> (Jy)	unc. (Jy)	bkgd <sub>24</sub> <sup>d</sup> (M Jy/sr)	unc. (M Jy/sr)
HD 127665	K 3III	0.582	0.028	1.773e+01	1.06e+00	4.187e+00	2.51e 01	4.631e+00	1.28e 01	2.15e+01	1.96e+00
HD 128620	G 2V	1.922	0.146					4.389e+01	6.50e+00	3.59e+01	4.50e+00
HD 128998	A 1V	5.757	0.013	1.139e 01	1.14e 02			3.534e 02	8.76e 04	1.70e+01	7.99e 01
HD 129078	K 2.5III	0.679	0.210	1.737e+01	5.21e 01	4.261e+00	1.28e 01	4.636e+00	1.05e 01	1.78e+01	3.49e+00
HD 129655	A 2	6.702	0.018					1.495e 02	4.25e 04	4.17e+01	9.95e+00
HD 131873	K 4III	1.359	0.141	1.137e+02	4.55e+00	2.693e+01	1.08e+00	2.974e+01	8.58e 01	1.56e+01	2.10e+00
HD 131986	K 0/K 1III	6.852	0.016					1.433e 02	3.93e 04	4.98e+01	4.79e+00
HD 132417	K 0/K 1III	6.388	0.013					2.197e 02	5.67e 04	4.74e+01	4.82e+00
HD 132439	K 2III	5.679	0.014					4.222e 02	1.11e 03	3.32e+01	4.88e+00
HD 134493	K 0III	3.922	0.120	8.047e 01	3.22e 02	1.775e 01	1.24e 02	2.083e 01	7.10e 03	1.68e+01	9.05e 01
HD 136422	K 5III	0.171	0.231	3.514e+01	1.41e+00	8.305e+00	4.15e 01	9.214e+00	2.93e 01	3.61e+01	9.21e+00
HD 137759	K 2III	0.584	0.028	1.634e+01	6.54e 01	4.026e+00	1.61e 01	4.464e+00	1.02e 01	1.61e+01	1.25e+00
HD 138265	K 5III	1.523	0.177	3.644e+00	1.09e 01	9.313e 01	3.72e 02	9.848e 01	2.46e 02	1.60e+01	1.39e+00
HD 139063	K 5III	0.227	0.230	2.145e+01	1.07e+00	5.265e+00	3.16e 01	5.723e+00	0.221e 01	4.52e+01	1.24e+01
HD 139698	G 8/K 0III	7.136	0.019					1.103e 02	3.23e 04	4.62e+01	5.78e+00
HD 140573	K 2IIIB	0.036	0.028	2.850e+01	1.14e+00	7.028e+00	4.22e 01	7.836e+00	1.94e 01	2.99e+01	6.06e+00
HD 141477	M 0.5III	0.016	0.028	3.110e+01	1.55e+00	7.606e+00	3.80e 01	8.139e+00	2.07e 01	2.36e+01	3.83e+00
HD 141937	G 2.5V	5.772	0.013	1.221e 01	1.71e 02			3.649e 02	1.01e 03	5.05e+01	1.40e+01
HD 144873	G 5	6.913	0.013					1.283e 02	3.63e 04	1.86e+01	2.16e+00
HD 145829	K 2III	5.142	0.018					6.923e 02	1.98e 03	6.27e+01	6.67e+00
HD 146051	M 0.5III	1.281	0.028	1.077e+02	5.38e+00	2.600e+01	1.30e+00	2.693e+01	6.87e 01	3.69e+01	8.99e+00
HD 149447	K 6III	0.356	0.226					5.685e+00	1.29e+00	4.21e+01	1.13e+01
HD 150039	K 0III	4.872	0.013					8.878e 02	2.29e 03	6.09e+01	8.06e+00
HD 150680	G 0IV	1.174	0.183	9.061e+00	4.53e 01	2.246e+00	1.35e 01	2.447e+00	9.38e 02	1.87e+01	2.68e+00
HD 150706	G 0	5.559	0.018	1.571e 01	9.42e 03			4.401e 02	1.21e 03	1.58e+01	2.30e+00
HD 150798	K 2II-III	1.140	0.133	1.036e+02	3.11e+00	2.355e+01	7.06e 01	2.655e+01	5.95e 01	2.04e+01	4.43e+00
HD 151249	K 5III	0.039	0.242					8.179e+00	1.99e+00	2.40e+01	5.54e+00
HD 151680	K 2.5III	0.389	0.140					1.129e+01	1.60e+00	4.35e+01	1.19e+01
HD 152222	K 2III	3.748	0.150	1.365e+00	8.19e 02	3.077e 01	1.85e 02	3.362e 01	1.40e 02	1.53e+01	2.00e+00
HD 153210	K 2III	0.549	0.028	1.735e+01	8.68e 01	4.033e+00	2.02e 01	4.635e+00	1.18e 01	2.60e+01	5.51e+00
HD 153458	G 0	6.456	0.013					1.955e 02	5.52e 04	3.98e+01	1.02e+01
HD 154391	K 2III	4.032	0.111	7.627e 01	2.29e 02	1.923e 01	9.61e 03	2.030e 01	5.28e 03	1.50e+01	2.02e+00
HD 156283	K 3Iab	0.012	0.028	3.320e+01	1.33e+00	7.700e+00	3.85e 01	8.321e+00	1.99e 01	1.74e+01	2.71e+00
HD 158460	A 2V	5.489	0.013	1.610e 01	8.05e 03			4.529e 02	1.03e 03	1.53e+01	2.04e+00
HD 158485	A 4V	6.136	0.016	7.908e 02	8.70e 03			2.489e 02	6.59e 04	1.50e+01	1.76e+00
HD 159048	K 0III	4.122	0.236	8.951e 01	2.68e 02	2.302e 01	1.15e 02	2.391e 01	6.36e 03	1.56e+01	1.98e+00
HD 159222	G 5V	4.977	0.013	2.604e 01	1.56e 02			7.483e 02	1.92e 03	1.77e+01	2.99e+00
HD 159330	K 2III	2.867	0.146	2.065e+00	6.19e 02	4.976e 01	1.99e 02	5.467e 01	1.35e 02	1.49e+01	1.71e+00
HD 161096	K 2III	0.129	0.028	2.645e+01	1.32e+00	6.129e+00	3.06e 01	6.943e+00	1.77e 01	2.81e+01	6.63e+00
HD 161743	B 9IV	7.585	0.018					6.630e 03	1.89e 04	4.07e+01	1.10e+01
HD 163376	M 0III	0.748	0.229					3.962e+00	9.12e 01	3.65e+01	9.80e+00
HD 163466	A 2V	6.364	0.013	8.919e 02	1.07e 02			2.053e 02	5.14e 04	1.53e+01	2.16e+00
HD 163588	K 2III	0.971	0.028	1.165e+01	3.49e 01	2.853e+00	8.56e 02	3.142e+00	6.02e 02	1.49e+01	1.82e+00
HD 164058	K 5III	1.408	0.028	1.106e+02	3.32e+00	2.713e+01	8.14e 01	2.931e+01	5.62e 01	1.56e+01	2.38e+00
HD 165459	A 2?	6.604	0.027	7.533e 02	1.20e 02			1.649e 02	5.62e 04	1.54e+01	2.21e+00
HD 166780	K 4.5III	3.792	0.101	7.866e 01	3.15e 02	1.919e 01	1.34e 02	2.104e 01	7.07e 03	1.49e+01	1.88e+00
HD 167389	F 8	5.908	0.015	1.118e 01	1.01e 02			3.210e 02	8.93e 04	1.66e+01	2.94e+00
HD 169916	K 1IIIB	0.298	0.028					5.997e+00	2.15e 01	5.08e+01	1.36e+01
HD 170693	K 1.5III	2.147	0.159	5.002e+00	1.50e 01	1.187e+00	3.56e 02	1.311e+00	2.95e 02	1.53e+01	2.31e+00
HD 172066	G 5?	6.279	0.015	8.687e 02	8.69e 03			2.302e 02	6.46e 04	1.54e+01	2.35e+00
HD 172728	A 0V	5.748	0.013	1.326e 01	1.06e 02			3.602e 02	8.78e 04	1.53e+01	2.36e+00
HD 173398	K 0III	4.003	0.213	8.061e 01	3.22e 02	1.912e 01	1.15e 02	2.120e 01	7.13e 03	1.54e+01	2.38e+00
HD 173511	K 5III	3.892	0.134	8.253e 01	2.48e 02	1.945e 01	9.73e 03	2.163e 01	5.67e 03	1.54e+01	2.39e+00
HD 173976	K 5III	3.572	0.177	1.186e+00	3.56e 02	2.966e 01	1.19e 02	3.163e 01	7.87e 03	1.53e+01	2.43e+00
HD 174123	G 5?	6.587	0.014	5.984e 02	8.98e 03			1.727e 02	4.87e 04	1.54e+01	2.39e+00
HD 175510	A 0V	4.960	0.124	2.920e 01	2.04e 02			7.833e 02	4.82e 03	2.76e+01	6.66e+00
HD 176841	G 5?	6.121	0.016	9.380e 02	1.22e 02			2.652e 02	7.69e 04	1.54e+01	2.44e+00
HD 177716	K 1IIIB	0.495	0.213	1.861e+01	9.30e 01	4.201e+00	2.10e 01	4.785e+00	1.71e 01	4.97e+01	1.38e+01
HD 180093	K 0Iab	5.081	0.015	5.662e+01	2.83e+00	1.862e+01	9.31e 01	7.340e 02	1.97e 03	4.44e+01	1.25e+01
HD 180711	G 9III	0.734	0.028	1.495e+01	4.49e 01	3.583e+00	1.08e 01	3.974e+00	7.62e 02	1.52e+01	2.74e+00
HD 181655	G 8V	4.625	0.013	3.838e 01	2.30e 02	9.729e 02	1.46e 02	1.097e 01	2.57e 03	1.73e+01	3.43e+00
HD 183439	M 0III	0.478	0.028					5.081e+00	1.82e 01	2.15e+01	4.37e+00
HD 186791	K 3II	0.572	0.028					1.336e+01	4.78e 01	2.60e+01	6.18e+00
HD 189276	K 5Iab	0.785	0.168	9.434e+00	3.77e 01	2.417e+00	9.67e 02	2.581e+00	7.50e 02	1.54e+01	2.64e+00
HD 191854	G 5	5.808	0.015					3.551e 02	1.04e 03	1.92e+01	3.13e+00
HD 193017	F 8	5.949	0.013	1.381e 01	1.93e 02			3.134e 02	8.69e 04	3.73e+01	1.05e+01
HD 195034	G 5	5.547	0.017					4.516e 02	1.37e 03	2.14e+01	4.83e+00
HD 197989	K 0III	0.047	0.028					7.556e+00	2.70e 01	1.89e+01	3.86e+00
HD 198542	M 0III	0.209	0.198	2.784e+01	1.39e+00	6.685e+00	3.34e 01	7.318e+00	0.261e 01	4.70e+01	1.30e+01
HD 199598	G 0V	5.449	0.015	1.923e 01	1.54e 02			4.961e 02	1.36e 03	2.08e+01	4.47e+00
HD 200914	K 5/M 0III	0.513	0.185	2.049e+01	1.23e+00	5.094e+00	3.06e 01	5.466e+00	2.30e 01	4.78e+01	1.32e+01
HD 201941	A 2	6.634	0.016					1.592e 02	4.33e 04	3.36e+01	8.94e+00
HD 204277	F 8V	5.416	0.015	2.114e 01	2.32e 02			5.124e 02	1.45e 03	2.54e+01	5.90e+00
HD 205772	A 5IV	7.651	0.013					6.239e 03	1.60e 04	3.13e+01	7.06e+00

TABLE 5 | Continued

Name	Spectral Type	super- $K_s^a$ (mag.)	unc. (mag.)	f (12 m) <sup>b</sup>			f (25 m) <sup>b</sup>			predictions			
				f (Jy)	unc. (Jy)	f (Jy)	unc. (Jy)	f (24 m) <sup>c</sup> (Jy)	unc. (Jy)	bkgd <sub>24</sub> <sup>d</sup> (M Jy/sr)	unc. (M Jy/sr)		
HD 205905	G 4V	5.325	0.018	2.481e 01	2.98e 02					5.587e 02	1.67e 03	4.36e+ 01	1.15e+ 01
HD 209750	G 2Ib	0.917	0.028	1.383e+ 01	8.30e 01	3.014e+ 00	1.81e 01	3.430e+ 00	9.46e 02	4.08e+ 01	1.12e+ 01		
HD 209952	B 7IV	2.003	0.213	3.743e+ 00	1.50e 01	8.486e 01	5.09e 02	1.014e+ 00	3.42e 02	2.64e+ 01	5.30e+ 00		
HD 211416	K 3III	0.330	0.183	4.280e+ 01	1.71e+ 00	1.024e+ 01	4.10e 01	1.128e+ 01	3.28e 01	2.12e+ 01	3.80e+ 00		
HD 212291	G 5	6.263	0.020					2.335e 02	7.49e 04	3.29e+ 01	8.06e+ 00		
HD 213310	M 0II+	0.158	0.028					6.822e+ 00	2.44e 01	1.76e+ 01	2.76e+ 00		
HD 216032	K 5III	0.167	0.028	2.674e+ 01	1.60e+ 00	6.646e+ 00	3.99e 01	6.923e+ 00	1.91e 01	4.98e+ 01	1.35e+ 01		
HD 216131	G 8II	1.374	0.028	8.362e+ 00	5.02e 01	1.989e+ 00	1.19e 01	2.217e+ 00	6.11e 02	2.51e+ 01	4.94e+ 00		
HD 216275	G 0	5.782	0.013					3.637e 02	1.03e 03	1.77e+ 01	2.94e+ 00		
HD 217014	G 2.5I	3.873	0.028	7.502e 01	4.50e 02	1.715e 01	2.23e 02	2.137e 01	6.42e 03	2.74e+ 01	5.67e+ 00		
HD 217382	K 4III	1.471	0.193	8.334e+ 00	2.50e 01	1.936e+ 00	1.36e 01	2.176e+ 00	6.15e 02	1.75e+ 01	2.66e+ 00		
HD 217906	M 2.5II	2.190	0.028	2.702e+ 02	1.35e+ 01	6.888e+ 01	3.44e+ 00	6.472e+ 01	1.66e+ 00	2.41e+ 01	4.45e+ 00		
HD 60178J	A 2V	1.431	0.028	7.211e+ 00	4.33e 01	1.624e+ 00	8.12e 02	1.893e+ 00	5.01e 02	4.50e+ 01	1.22e+ 01		
HD 98230J	G 0V	2.090	0.187	4.069e+ 00	2.03e 01	8.779e 01	5.27e 02	1.036e+ 00	3.98e 02	3.15e+ 01	5.37e+ 00		
NPM 1+ 61.0569	K 0.5III	7.210	0.013					1.031e 02	2.66e 04	1.53e+ 01	2.04e+ 00		
NPM 1+ 68.0412	K 2III	7.169	0.015					1.070e 02	2.87e 04	1.54e+ 01	2.34e+ 00		
SAO 9310	K 0	7.332	0.014					9.211e 03	2.42e 04	1.58e+ 01	2.41e+ 00		

<sup>a</sup> Super- $K_s$  is the weighted average of J (transformed to  $K_s$ ) and  $K_s$  (see x 4.1).

<sup>b</sup> Taken from the IRAS Faint Source Catalog, and modified as discussed in x 4.1.3.

<sup>c</sup> These flux densities apply to the effective wavelength of the 24 m band, 23.675 m.

<sup>d</sup> See x 4.3.

TABLE 6  
Combined Measurements and Calibration Factors

Name	number of measurements	24 m count rate <sup>a</sup> (DN/s)	uncertainty (DN/s)	calibration factor (M Jy/sr/DN/s)	uncertainty (M Jy/sr/DN/s)
BD + 621644	1	1.033e+04	5.19e+01	4.037e-02	9.72e-04
HD 000319	1	6.708e+03	5.00e+01	4.262e-02	1.16e-03
HD 001160	1	1.395e+03	1.56e+01	5.250e-02	1.60e-03
HD 001644	1	8.191e+03	5.69e+01	4.534e-02	1.25e-03
HD 002151	1	3.271e+05	1.23e+03	4.573e-02	1.46e-03
HD 002811	1	1.591e+03	3.35e+01	4.331e-02	1.51e-03
HD 008941	1	7.202e+03	3.46e+01	4.948e-02	1.40e-03
HD 009927	1	6.045e+05	2.45e+03	4.539e-02	1.17e-03
HD 011413	1	7.866e+03	3.87e+01	3.856e-02	9.81e-04
HD 014943	1	7.180e+03	2.84e+01	4.192e-02	1.14e-03
HD 015008	5	2.719e+04	1.21e+01	4.757e-02	1.67e-03
HD 015646	1	2.997e+03	4.84e+01	4.349e-02	1.36e-03
HD 017254	5	4.622e+03	1.02e+01	4.368e-02	1.10e-03
HD 019019	1	6.204e+03	3.74e+01	4.714e-02	1.41e-03
HD 020722	1	5.818e+03	4.56e+01	3.517e-02	9.62e-04
HD 020888	2	5.519e+03	2.04e+01	4.407e-02	1.19e-03
HD 020902	1	6.872e+05	2.62e+03	4.361e-02	1.56e-03
HD 021981	1	6.089e+03	1.33e+01	4.447e-02	1.22e-03
HD 025860	1	4.202e+03	3.26e+01	4.031e-02	1.08e-03
HD 027466	1	3.146e+03	3.18e+01	4.846e-02	1.46e-03
HD 028099	1	2.546e+03	2.80e+01	4.635e-02	1.47e-03
HD 028471	1	3.173e+03	1.81e+01	4.590e-02	1.39e-03
HD 029461	1	2.759e+03	2.77e+01	4.736e-02	1.62e-03
HD 030246	1	2.497e+03	2.75e+01	4.011e-02	1.38e-03
HD 032831	1	2.301e+05	8.06e+02	4.509e-02	8.79e-04
HD 034868	1	3.851e+03	3.89e+01	4.791e-02	1.46e-03
HD 035666	1	3.416e+04	1.34e+02	4.578e-02	1.52e-03
HD 036167	1	5.627e+05	2.23e+03	4.301e-02	2.54e-03
HD 037962	1	3.281e+03	3.12e+01	4.565e-02	1.39e-03
HD 038949	1	2.871e+03	3.10e+01	4.602e-02	1.51e-03
HD 039608	6	3.861e+04	1.25e+01	4.455e-02	1.46e-03
HD 040129	1	2.025e+03	2.04e+01	4.609e-02	1.43e-03
HD 040335	1	2.866e+03	3.25e+01	4.383e-02	1.27e-03
HD 041371	4	1.498e+04	1.16e+01	4.373e-02	1.00e-03
HD 042525	1	5.116e+03	2.85e+01	4.460e-02	1.14e-03
HD 042701	2	4.346e+04	1.20e+02	4.515e-02	8.27e-04
HD 043107	14	8.368e+03	1.16e+01	4.660e-02	1.07e-03
HD 044594	1	9.411e+03	4.79e+01	4.631e-02	1.30e-03
HD 045557	1	5.492e+03	3.51e+01	4.228e-02	1.06e-03
HD 046190	1	3.703e+03	2.82e+01	3.518e-02	9.61e-04
HD 046819	1	8.504e+03	4.94e+01	4.627e-02	1.15e-03
HD 047332	1	2.595e+03	2.60e+01	3.852e-02	1.05e-03
HD 050310	1	7.865e+05	2.88e+03	5.228e-02	1.54e-03
HD 053501	4	1.838e+05	3.71e+02	4.531e-02	1.03e-03
HD 057336	1	1.403e+03	3.44e+01	4.446e-02	1.71e-03
HD 058142	1	1.458e+04	1.33e+02	4.686e-02	2.57e-03
HD 060178	1	2.584e+05	7.17e+02	4.808e-02	1.28e-03
HD 061929	1	3.038e+03	2.66e+01	4.569e-02	1.35e-03
HD 064324	1	3.672e+03	3.87e+01	4.256e-02	1.28e-03
HD 065517	1	2.122e+03	1.81e+01	3.928e-02	1.19e-03
HD 066751	1	9.671e+03	2.80e+01	4.704e-02	1.30e-03
HD 069863	1	1.240e+04	5.52e+01	4.140e-02	9.15e-04
HD 073210	1	3.707e+03	5.55e+01	4.261e-02	1.30e-03
HD 073666	1	2.541e+03	5.66e+01	4.584e-02	1.59e-03
HD 073819	1	3.170e+03	5.29e+01	4.553e-02	1.41e-03
HD 077281	1	1.673e+03	1.99e+01	4.374e-02	1.30e-03
HD 080007	2	2.594e+05	6.64e+02	4.536e-02	1.33e-03
HD 082308	1	7.022e+05	2.59e+03	4.484e-02	1.32e-03
HD 082621	1	1.909e+04	8.24e+01	4.679e-02	2.47e-03
HD 087901	1	2.350e+05	7.87e+02	4.929e-02	1.39e-03
HD 091375	1	1.602e+04	6.73e+01	4.646e-02	2.18e-03
HD 092788	1	5.299e+03	3.93e+01	4.713e-02	1.64e-03
HD 092845	1	7.166e+03	4.51e+01	3.975e-02	1.08e-03
HD 096833	2	7.426e+05	2.07e+03	4.910e-02	1.26e-03
HD 098230	1	1.467e+05	4.65e+02	4.635e-02	1.78e-03
HD 098553	1	3.858e+03	3.39e+01	4.732e-02	1.41e-03
HD 100167	1	5.036e+03	3.57e+01	4.587e-02	1.36e-03
HD 101452	1	1.910e+03	3.50e+01	4.292e-02	1.45e-03
HD 101472	1	3.834e+03	3.44e+01	4.534e-02	1.41e-03
HD 101959	1	5.822e+03	3.20e+01	4.755e-02	1.38e-03
HD 102647	2	2.365e+05	5.09e+02	3.519e-02	1.08e-03
HD 102870	1	1.309e+05	5.02e+02	4.834e-02	3.18e-03
HD 105805	1	5.734e+03	5.10e+01	4.692e-02	1.52e-03
HD 106252	1	4.749e+03	3.73e+01	4.326e-02	1.35e-03
HD 106965	1	1.248e+03	1.87e+01	4.533e-02	1.43e-03

TABLE 6 | Continued

Nam e	num ber of m easurem ents	24 m count rate <sup>a</sup> (DN /s)	uncertainty (DN /s)	calibration factor (M Jy/sr/ DN /s)	uncertainty (M Jy/sr/ DN /s)
HD 108799	1	1.242e+ 04	4.16e+ 01	4.490e 02	1.28e 03
HD 108944	1	4.431e+ 03	3.10e+ 01	4.443e 02	1.25e 03
HD 109612	1	1.260e+ 04	6.56e+ 01	3.864e 02	1.04e 03
HD 109866	1	4.368e+ 03	2.77e+ 01	9.297e 02	2.62e 03
HD 110304	1	1.510e+ 05	5.70e+ 02	4.672e 02	1.20e 03
HD 112196	1	6.345e+ 03	3.41e+ 01	4.660e 02	1.39e 03
HD 115043	1	7.863e+ 03	3.29e+ 01	4.500e 02	1.26e 03
HD 115780	2	1.041e+ 04	9.28e+ 01	1.592e 02	4.59e 04
HD 116706	1	6.188e+ 03	5.01e+ 01	4.846e 02	1.33e 03
HD 119545	1	1.360e+ 05	2.33e+ 03	1.412e 03	4.37e 05
HD 121370	1	3.132e+ 05	1.17e+ 03	4.878e 02	1.80e 03
HD 121504	1	4.016e+ 03	4.34e+ 01	4.169e 02	2.27e 03
HD 122652	1	5.100e+ 03	2.87e+ 01	4.378e 02	1.28e 03
HD 123123	1	6.343e+ 05	2.39e+ 03	4.503e 02	1.20e 03
HD 127665	1	6.687e+ 05	2.51e+ 03	4.545e 02	1.26e 03
HD 128998	1	4.824e+ 03	2.79e+ 01	4.808e 02	1.22e 03
HD 129655	1	2.577e+ 03	2.87e+ 01	3.807e 02	1.16e 03
HD 131986	1	7.721e+ 03	9.91e+ 01	1.218e 02	3.69e 04
HD 132417	1	5.041e+ 03	5.49e+ 01	2.860e 02	8.01e 04
HD 132439	1	5.055e+ 03	3.77e+ 01	5.481e 02	1.50e 03
HD 134493	1	2.956e+ 04	1.24e+ 02	4.625e 02	1.59e 03
HD 138265	2	1.446e+ 05	4.23e+ 02	4.470e 02	1.12e 03
HD 139698	1	8.006e+ 03	1.99e+ 02	9.042e 03	3.47e 04
HD 141937	1	5.126e+ 03	3.82e+ 01	4.672e 02	1.34e 03
HD 144873	1	1.723e+ 03	1.96e+ 01	4.887e 02	1.49e 03
HD 150680	1	3.335e+ 05	1.33e+ 03	4.815e 02	1.86e 03
HD 150706	1	6.656e+ 03	3.12e+ 01	4.339e 02	1.21e 03
HD 152222	3	5.150e+ 04	1.92e+ 01	4.284e 02	1.79e 03
HD 153458	1	2.799e+ 03	3.91e+ 01	4.584e 02	1.44e 03
HD 154391	1	3.023e+ 04	1.22e+ 02	4.407e 02	1.16e 03
HD 158460	1	7.931e+ 03	5.71e+ 01	3.748e 02	8.97e 04
HD 158485	1	3.564e+ 03	2.80e+ 01	4.583e 02	1.27e 03
HD 159048	1	3.600e+ 04	1.88e+ 02	4.359e 02	1.18e 03
HD 159222	5	1.010e+ 04	1.02e+ 01	4.862e 02	1.25e 03
HD 159330	102	7.929e+ 04	1.65e+ 01	4.525e 02	1.12e 03
HD 163466	3	2.938e+ 03	1.90e+ 01	4.586e 02	1.19e 03
HD 163588	2	4.479e+ 05	1.34e+ 03	4.604e 02	8.93e 04
HD 165459	2	3.843e+ 03	2.48e+ 01	2.816e 02	9.77e 04
HD 166780	2	3.065e+ 04	8.84e+ 01	4.505e 02	1.52e 03
HD 167389	1	4.449e+ 03	2.66e+ 01	4.735e 02	1.35e 03
HD 170693	4	1.855e+ 05	2.14e+ 01	4.638e 02	1.04e 03
HD 172066	1	3.368e+ 03	2.68e+ 01	4.486e 02	1.31e 03
HD 172728	2	4.747e+ 03	2.21e+ 01	4.980e 02	1.24e 03
HD 173398	46	3.031e+ 04	1.84e+ 01	4.590e 02	1.54e 03
HD 173511	1	3.165e+ 04	1.24e+ 02	4.485e 02	1.19e 03
HD 173976	1	4.749e+ 04	1.72e+ 02	4.371e 02	1.10e 03
HD 174123	1	2.296e+ 03	2.39e+ 01	4.936e 02	1.48e 03
HD 176841	1	3.644e+ 03	2.79e+ 01	4.776e 02	1.43e 03
HD 180711	2	5.759e+ 05	1.47e+ 03	4.529e 02	8.76e 04
HD 183439	2	7.200e+ 05	2.64e+ 03	4.631e 02	1.67e 03
HD 189276	2	3.857e+ 05	1.02e+ 03	4.392e 02	1.28e 03
HD 191854	3	4.867e+ 03	1.97e+ 01	4.788e 02	1.41e 03
HD 193017	1	4.150e+ 03	3.86e+ 01	4.956e 02	1.45e 03
HD 195034	1	6.127e+ 03	3.33e+ 01	4.837e 02	1.49e 03
HD 199598	1	7.021e+ 03	3.60e+ 01	4.637e 02	1.30e 03
HD 201941	1	2.900e+ 03	2.79e+ 01	3.603e 02	1.04e 03
HD 204277	1	7.301e+ 03	2.83e+ 01	4.606e 02	1.31e 03
HD 205905	1	7.871e+ 03	3.42e+ 01	4.658e 02	1.41e 03
HD 209952	2	1.465e+ 05	3.74e+ 02	4.542e 02	1.54e 03
HD 212291	1	3.319e+ 03	3.19e+ 01	4.617e 02	1.55e 03
HD 216131	1	3.277e+ 05	1.24e+ 03	4.440e 02	1.24e 03
HD 216275	1	5.062e+ 03	4.07e+ 01	4.715e 02	1.39e 03
HD 217382	1	3.264e+ 05	1.18e+ 03	4.375e 02	1.25e 03
NPM 1+ 61.0569	1	1.510e+ 03	1.64e+ 01	4.481e 02	1.25e 03
NPM 1+ 68.0412	1	1.494e+ 03	1.67e+ 01	4.700e 02	1.37e 03
SAO 9310	1	1.069e+ 03	1.24e+ 01	5.655e 02	1.63e 03

<sup>a</sup> The count rates in this table can be converted to Jy by multiplying by the product of the aperture correction, calibration factor, and pixel area discussed in the text, or a factor of  $6:92 \times 10^{-6}$ .

TABLE 7  
Stars Rejected as 24  $\mu$ m Calibrators.

Name	Reason for Rejection
BD + 621644	calibration factor 12% low
HD 011413	calibration factor 18% low <sup>a</sup>
HD 020722	double source <sup>b</sup>
HD 046190	calibration factor 29% low <sup>c</sup>
HD 047332	calibration factor 18% low <sup>a</sup>
HD 065517	calibration factor 16% low <sup>a</sup>
HD 092845	double star
HD 102647	calibration factor 29% low <sup>c</sup>
HD 109612	bright, complex background
HD 109866	bright, complex background
HD 115780	bright, complex background
HD 119545	bright, complex background
HD 129655	calibration factor 19% low <sup>a</sup>
HD 131986	bright, complex background and nearby contaminating sources
HD 132417	bright, complex background and nearby contaminating sources
HD 132439	bright, complex background
HD 139698	bright, complex background
HD 158460	calibration factor 21% low <sup>c</sup>
HD 165459	calibration factor 61% low <sup>c</sup>
HD 201941	calibration factor 26% low <sup>d</sup>
SAO 9310	calibration factor 20% high

<sup>a</sup>NIR measurements indicate this star is reddened, so the predicted flux is likely low.

<sup>b</sup>There is a 24  $\mu$ m source 14<sup>00</sup> to the north of this star. SIMBAD does not indicate the star is part of a multiple system and the Spitzer Planning and Observation Tool (SPOT) does not indicate any asteroids in the field, so the source is likely a background galaxy.

<sup>c</sup>Su et al. (2006) find this source has a debris disk.

<sup>d</sup>This star is not known to be part of a multiple system and no asteroids were expected in the field, so this star likely has an infrared excess.

TABLE 8  
24  $\mu$ m Observations of Cohen et al. Template Stars

Name	observed		template prediction		observed / template	unc.
	f (24 $\mu$ m) (Jy)	unc. (Jy)	f (24 $\mu$ m) (Jy)	unc. (Jy)		
HD 032831	1.592e+ 00	5.58e 03	1.560e+ 00	5.99e 02	1.020	0.039
HD 053501	1.271e+ 00	2.57e 03	1.238e+ 00	1.08e 01	1.027	0.089
HD 163588	3.098e+ 00	9.27e 03	3.018e+ 00	1.06e 01	1.027	0.036
HD 189276	2.668e+ 00	7.06e 03	2.559e+ 00	8.31e 02	1.043	0.034
HD 138265	1.000e+ 00	2.93e 03	9.507e 01	3.25e 02	1.052	0.036
HD 036167	3.893e+ 00	1.54e 02	3.800e+ 00	1.27e 01	1.024	0.035
HD 170693	1.283e+ 00	1.48e 04	1.291e+ 00	4.57e 02	0.994	0.035
HD 009927	4.182e+ 00	1.69e 02	3.908e+ 00	2.94e 01	1.070	0.081
HD 134493	2.045e 01	8.58e 04	2.017e 01	6.90e 03	1.014	0.035

Note. | The star HD 020722 has a template and was observed at 24  $\mu$ m, but was not included in this comparison due to a nearby source at 24  $\mu$ m (cf. Table 7).

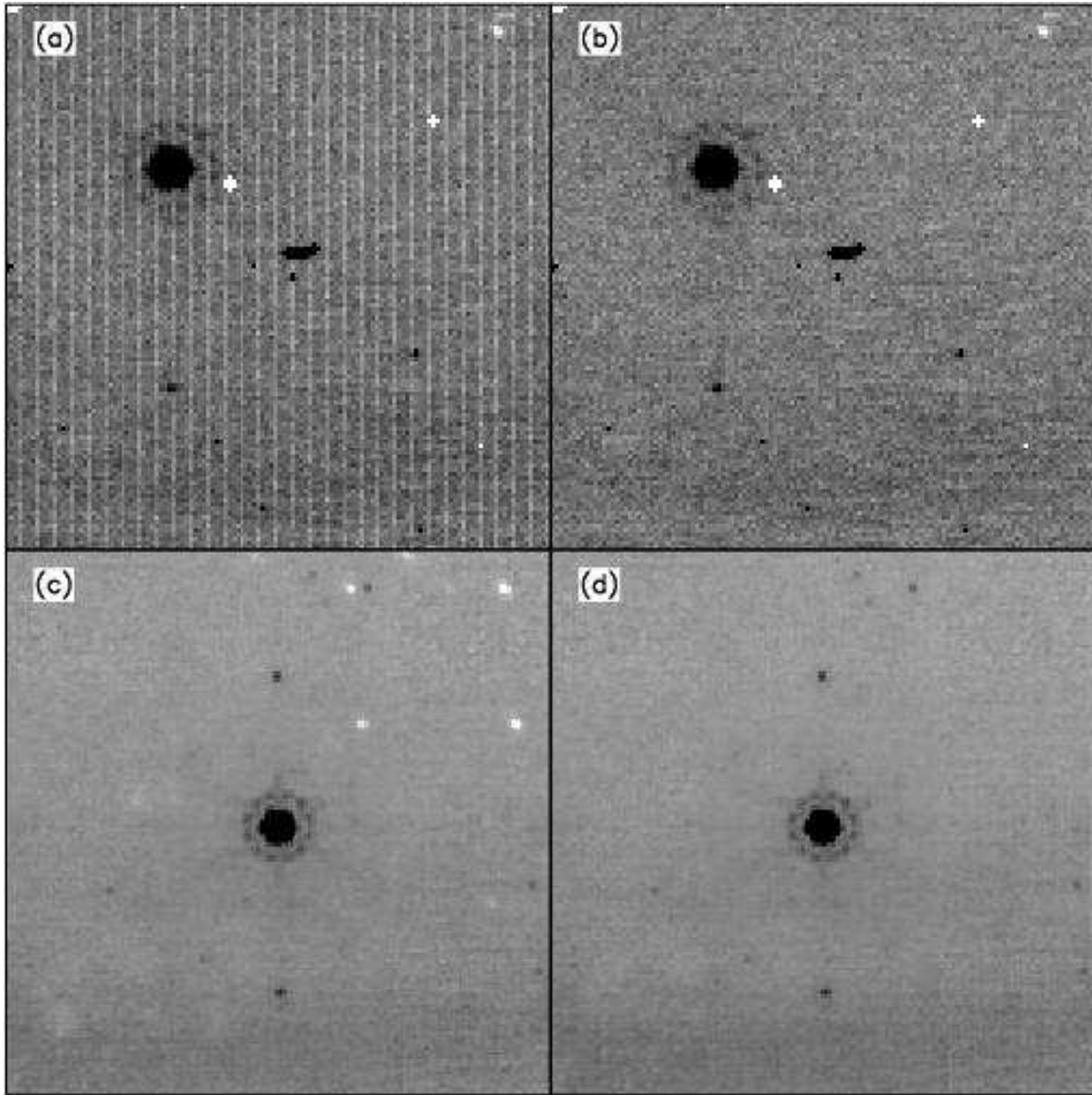


Fig. 1. | Artifacts not discussed by Gordon et al. (2005) that are now fixed as part of standard processing with the MIPS Data Analysis Tool (DAT), illustrated using observations of HD 159330 (AKRKEY 13587712) plotted in reverse grayscale. (a) The “jailbar” effect is most easily seen in individual frames, here caused by a cosmic ray below and to the right of the star, and (b) fixed as described in §2. (c) The spots caused by debris on the pick-off mirror (several sharp white spots above and to the right of the star, as well as diffuse white regions below and to the left of the star) are most easily seen in a mosaicked image and are (d) fixed using separate fields for each scan mirror position.



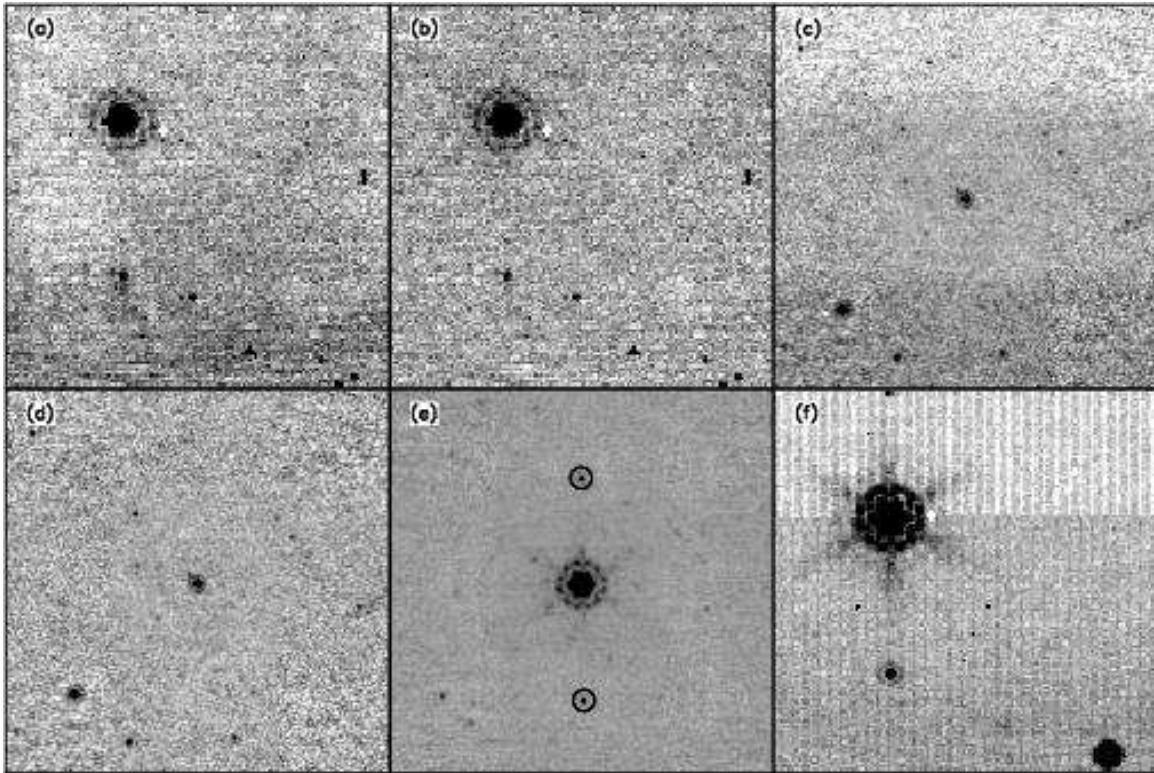


Fig. 2. | Artifacts not removed by standard processing with the MIPS Data Analysis Tool (DAT), plotted in reverse grayscale. As discussed in §2, (a) gain changes imposed by previous observations (illustrated using a single-frame observation of HD 159330, AORKEY 12195328) are (b) removed using a second standard. (c) Background changes as a function of scan mirror position (illustrated using a mosaic observation of HD 106965, AORKEY 13201920) are (d) removed before mosaicking. For the targets discussed here, the effects of (e) residual images (circled, illustrated using a mosaic observation of HD 159330, AORKEY 12195328) and (f) sources which saturate in 3 seconds (illustrated using a single-frame observation of HD 180711, AORKEY 9805568) are small and we make no correction.

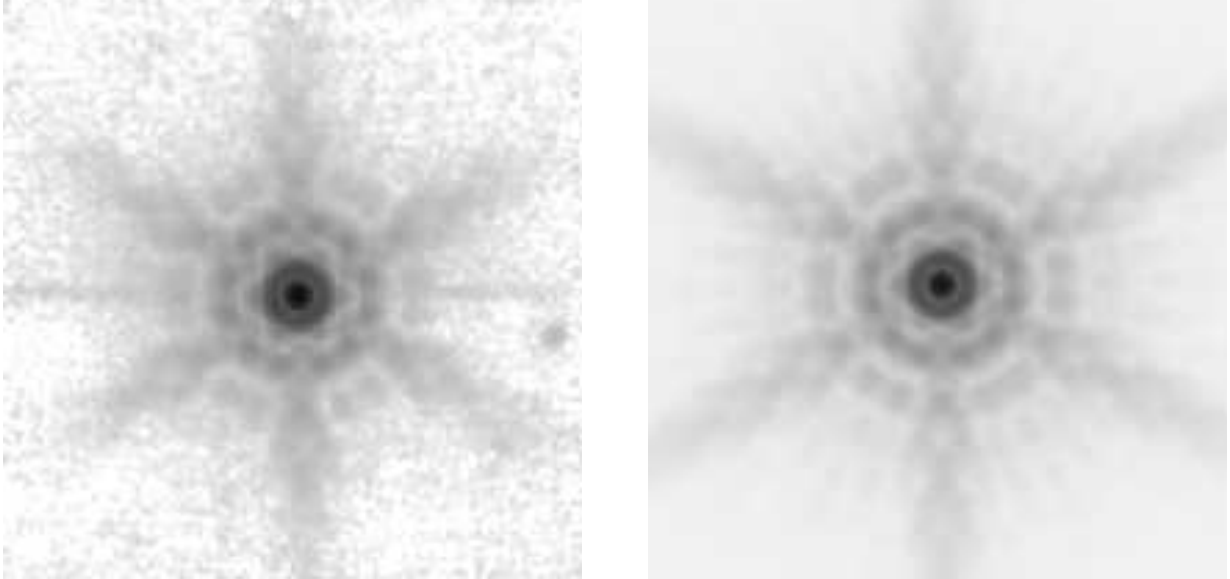


Fig. 3. Comparison of observed and model PSF, plotted in reverse grayscale. On the left is shown an image of HD 009927; the horizontal feature through the center of the image is a detector artifact. The dynamic range (from the peak brightness of 60,000 DN/s to the 1 $\sigma$  noise level of 3 DN/s) is 20,000. The image on the right is a model generated by StinyTin, after processing through the MIPS simulator (see x 2.4). Both images have been heavily compressed using an asinh transform to show faint structure and the grayscale levels have been adjusted by eye to match each other.

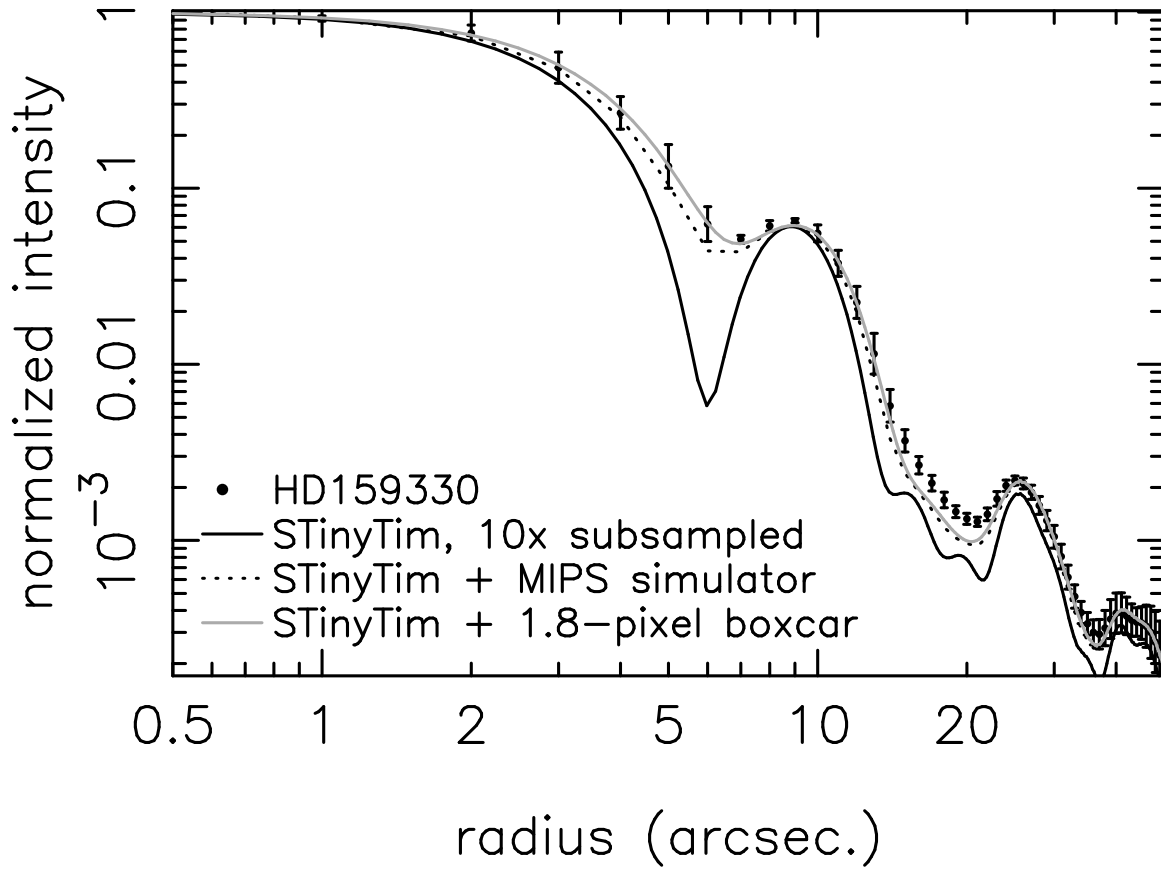


Fig. 4.1 The radial profile of a star (points), compared to a 10 $\times$  subsampled model profile generated by STinyTim (dark solid line), along with that same model profile run through the MIPS simulator (dark dotted line; see x2 for details) or smoothed by a 1.8-pixel boxcar (light solid line).

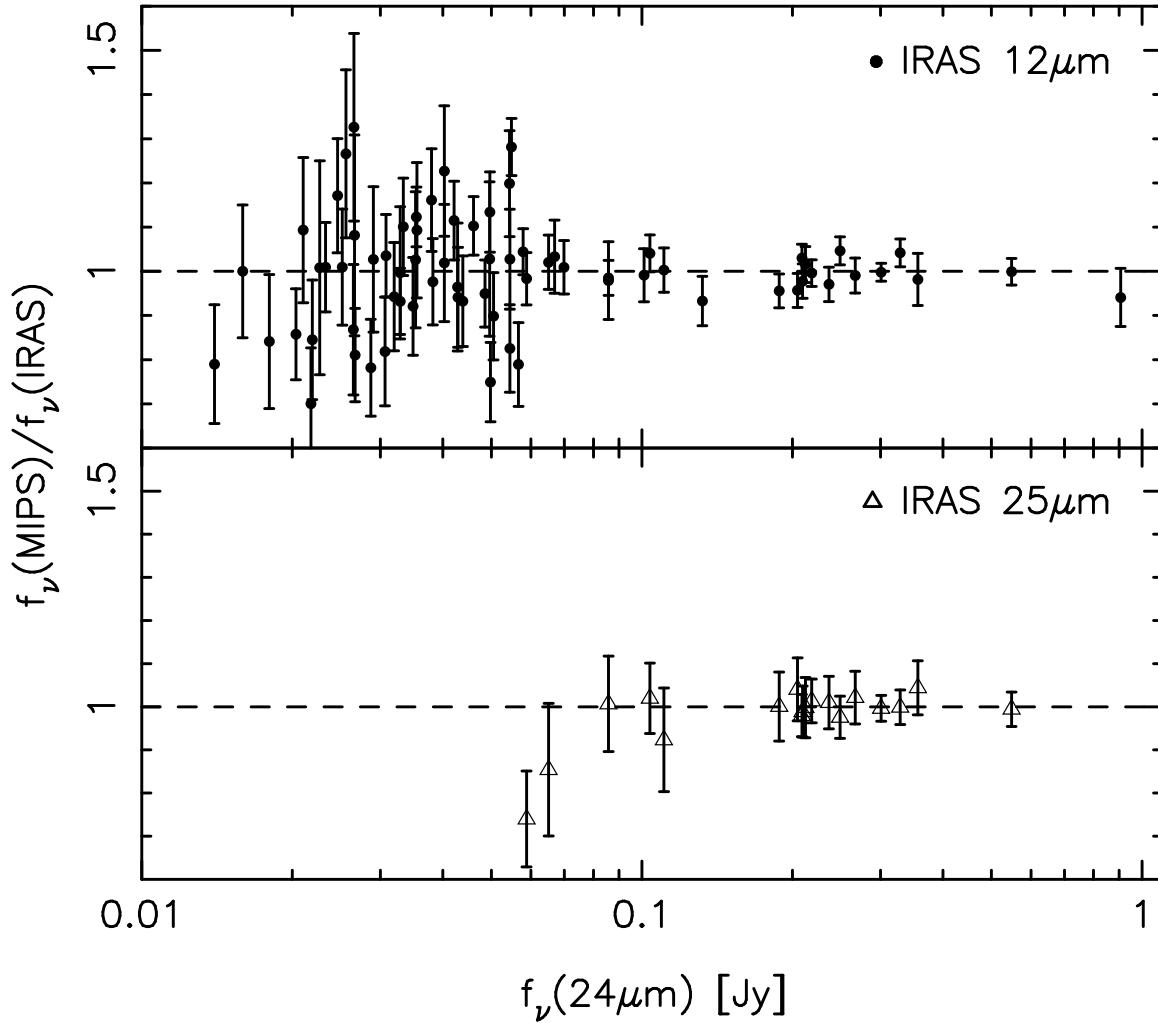


Fig. 5. | The ratio of MIPS 24  $\mu\text{m}$  flux densities to IRAS 12 and 25  $\mu\text{m}$  flux densities (filled circles and open triangles, respectively) as a function of 24  $\mu\text{m}$  flux density, normalized to the average ratios of 0.265 and 1.11, respectively. The error bars represent the combined IRAS and MIPS uncertainties. A dashed line is drawn at a ratio of 1 as a guide.

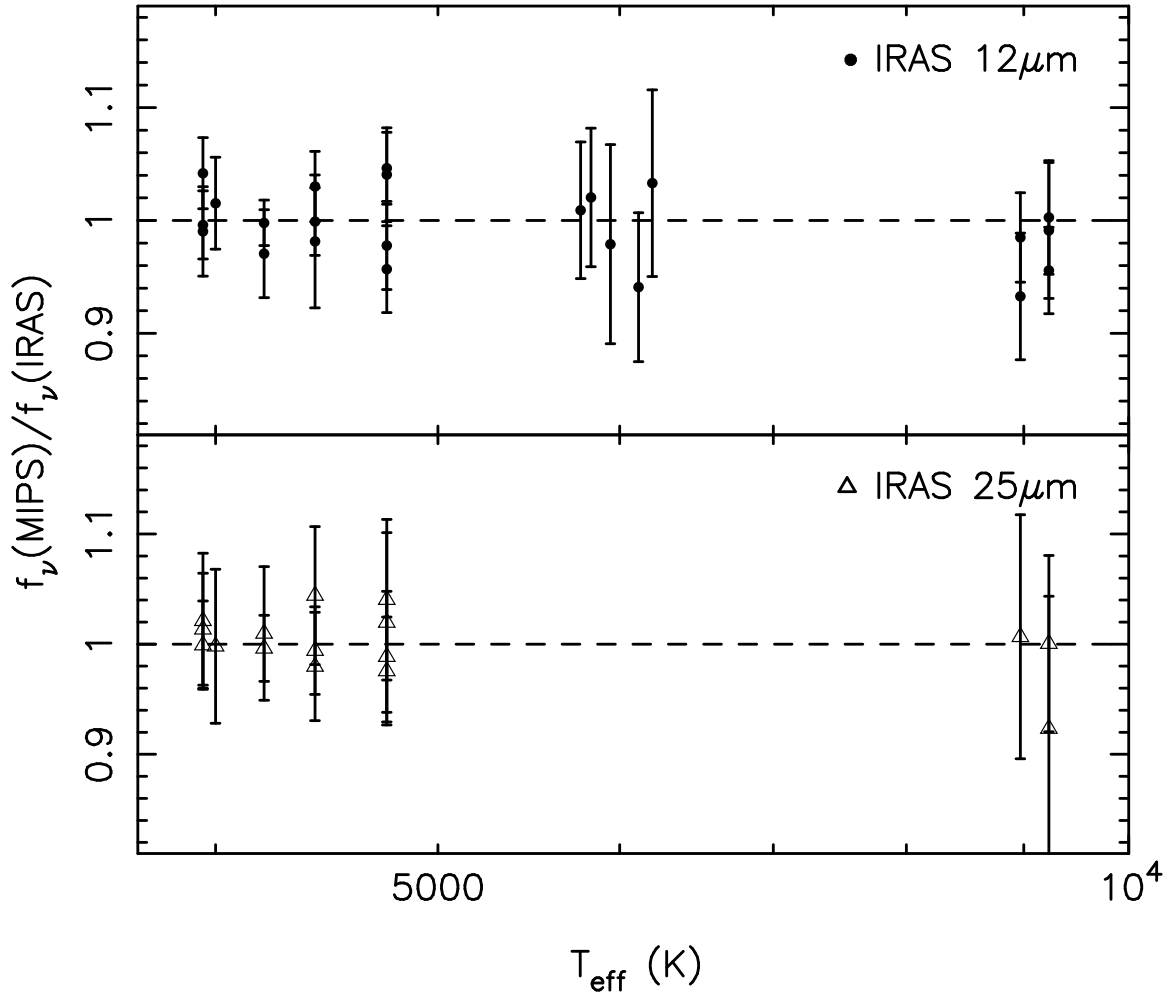


Fig. 6. | The ratio of MIPS 24  $\mu$ m flux densities to IRAS 12 and 25  $\mu$ m flux densities (filled circles and open triangles, respectively) as a function of spectral type, here quantified as the effective temperature of the star. The ratios have been normalized to the average ratios at 0.265 and 1.11 at 12 and 25  $\mu$ m. The error bars represent the combined IRAS and MIPS uncertainties. A dashed line is drawn at a ratio of 1 as a guide.

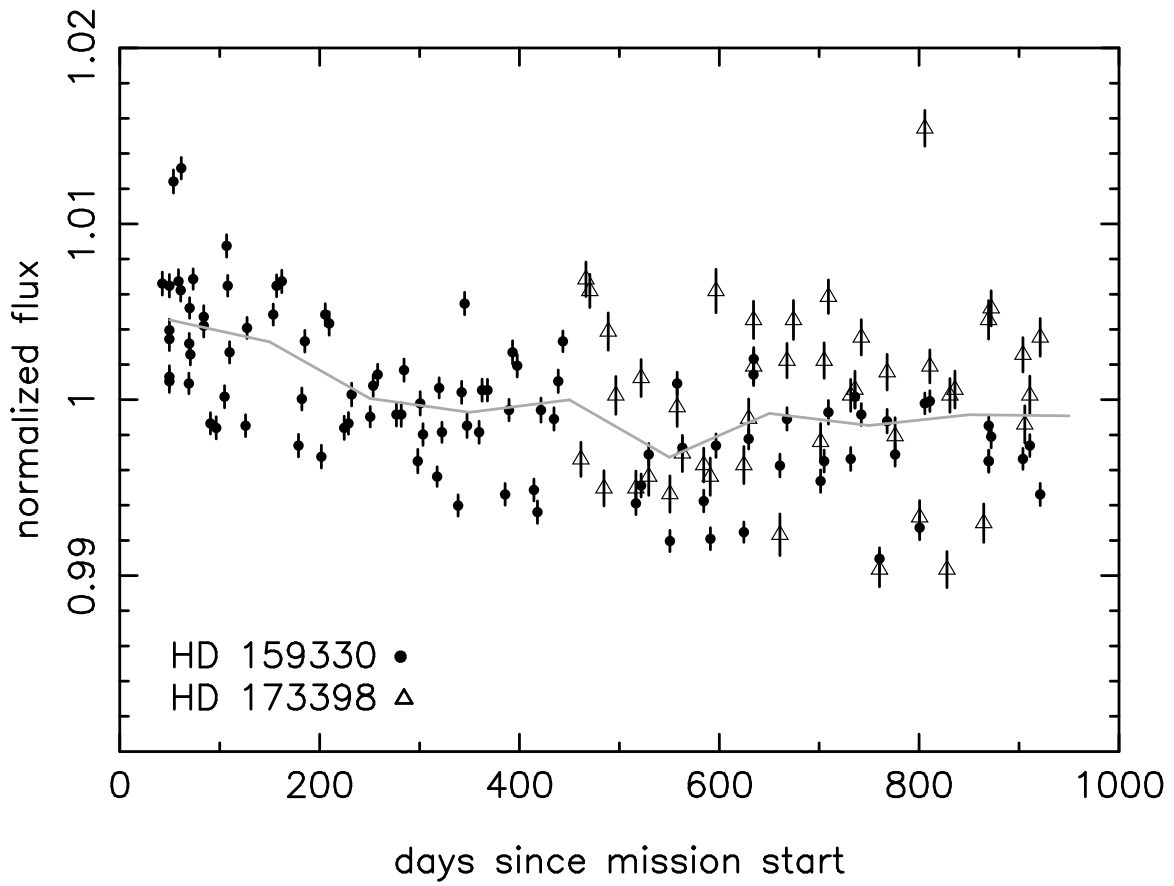


Fig. 7.] Repeatability of 24 m photometry on two routinely-monitored sources: HD 159330 (filled circles) and HD 173398 (open triangles). The gray curve is a sigma-a-clipped average in 10 equally-spaced bins.

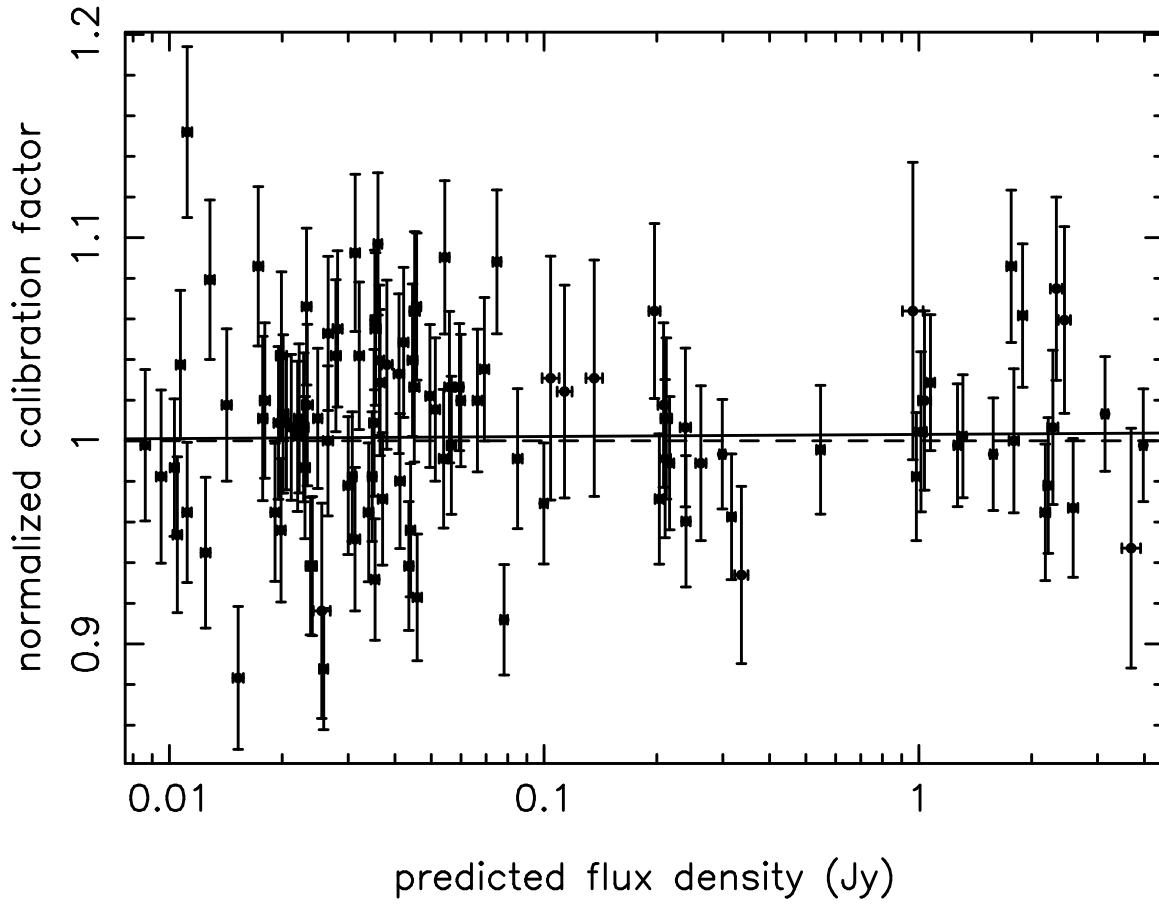


Fig. 8.1 24  $\mu$ m calibration factor normalized to the nominal calibration factor (see x 3) as a function of predicted 24  $\mu$ m flux density. The error bars are drawn from Tables 5 and 6. The dashed line is drawn at 1 as a guide, while the solid line is a linear least-squares fit to the data (see x 5). Points greater than 5% above or below the nominal calibration factor have been not been included in the plot or the fit.

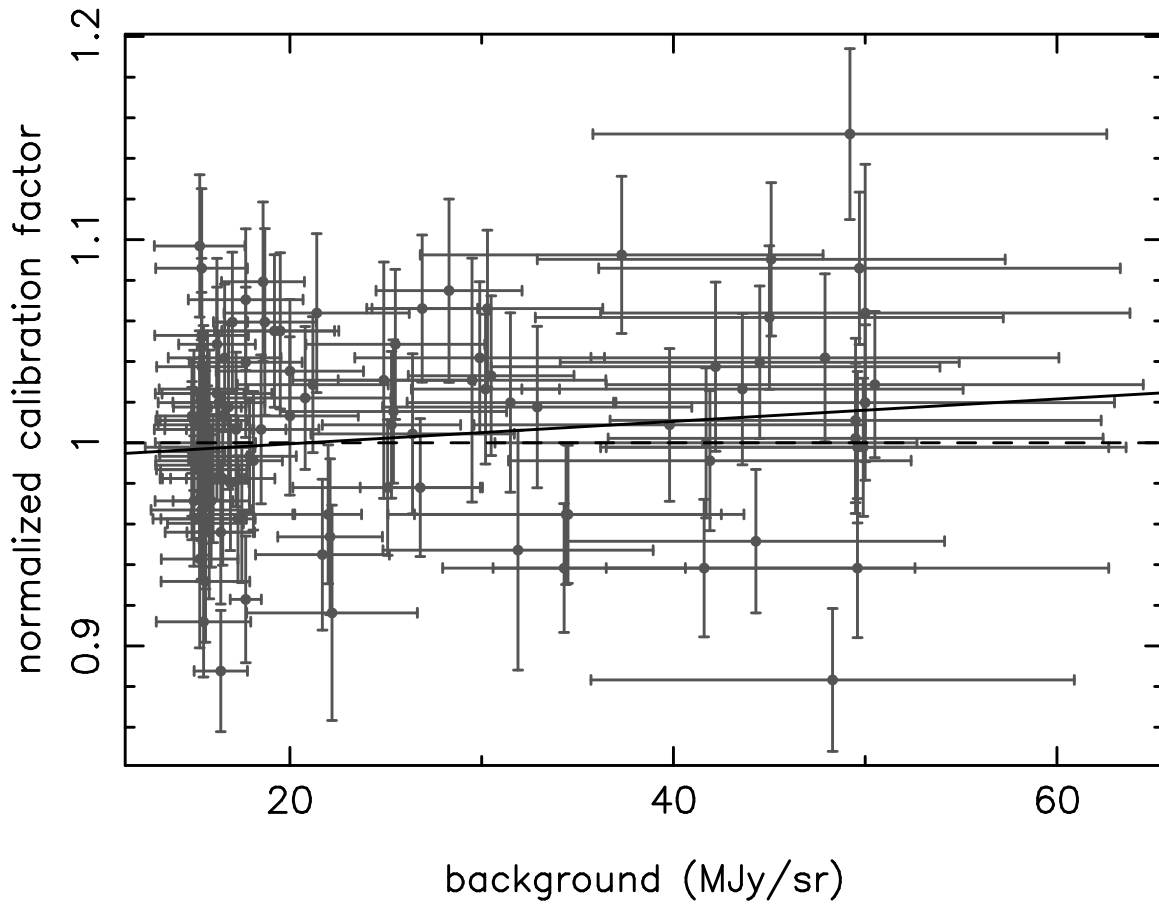


Fig. 9.1 24 m calibration factor normalized to the nominal calibration factor (see x 3) as a function of predicted background. The uncertainties represented by the error bars are drawn from Tables 5 and 6. The dashed line is drawn at 1 as a guide, while the solid line represents a linear least-squares fit to the data (see x 5). Points greater than 5% above or below the nominal calibration factor have been not been included in the plot or the fit.



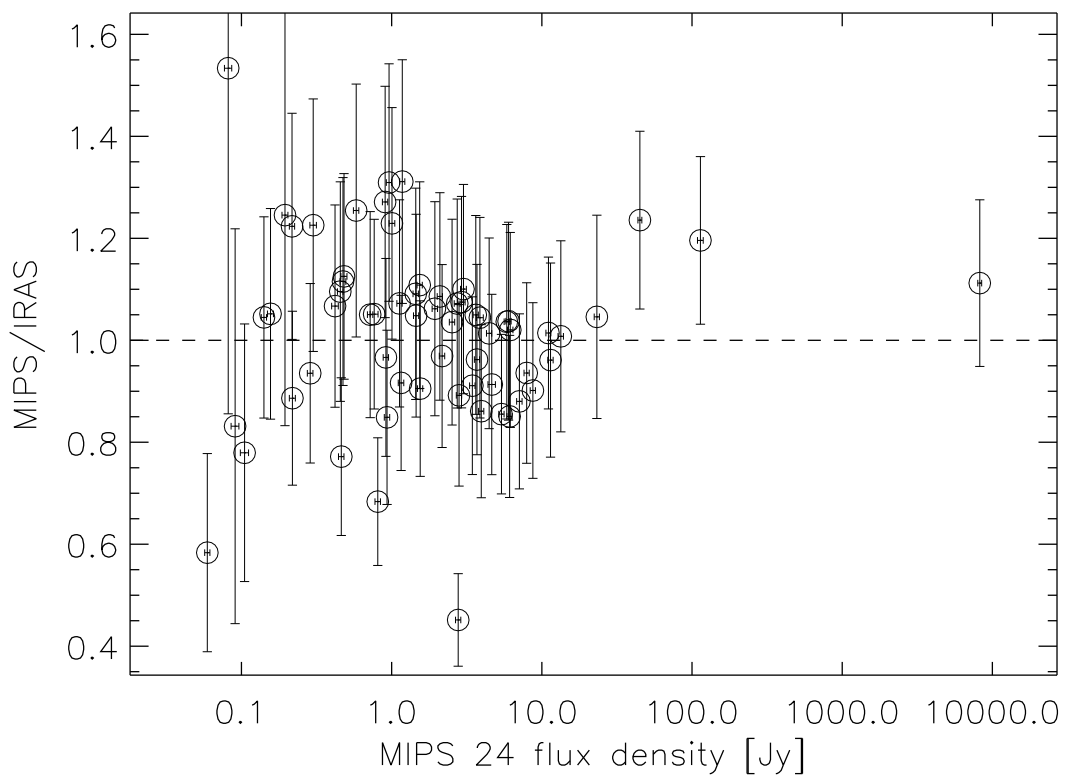


Fig. 10. | Ratio of MIPS to IRAS measurements of extended sources as a function of flux density measured at 24  $\mu$ m. The error bars represent the combined uncertainty on both measurements. The dashed line is drawn at 1 as a guide.